JGP Journal of General Physiology

ARTICLE

Excitation–Contraction Coupling

Constitutive assembly of Ca^{2+} entry units in soleus muscle from calsequestrin knockout mice

Antonio Michelucci[1,2], Laura Pietrangelo[1,3], Giorgia Rastelli[1], Feliciano Protasi[1,3], Robert T. Dirksen[4], and Simona Boncompagni[1,5]

Calcium (Ca^{2+}) entry units (CEUs) are junctions within the I band of the sarcomere between stacks of sarcoplasmic reticulum (SR) cisternae and extensions of the transverse (T)-tubule. CEUs contain STIM1 and Orai1 proteins, the molecular machinery of store-operated Ca^{2+} entry (SOCE). In extensor digitorum longus (EDL) fibers of wild-type (WT) mice, CEUs transiently assemble during acute exercise and disassemble several hours thereafter. By contrast, calsequestrin-1 (CASQ1) ablation induces a compensatory constitutive assembly of CEUs in EDL fibers, resulting in enhanced constitutive and maximum SOCE that counteracts SR Ca^{2+} depletion during repetitive activity. However, whether CEUs form in slow-twitch fibers, which express both the skeletal CASQ1 and the cardiac CASQ2 isoforms, is unknown. Herein, we compared the structure and function of soleus muscles from WT and knockout mice that lack either CASQ1 (CASQ1-null) or both CASQs (dCASQ-null). Ultrastructural analyses showed that SR/T-tubule junctions at the I band, virtually identical to CEUs in EDL muscle, were present and more frequent in CASQ1-null than WT mice, with dCASQ-null exhibiting the highest incidence. The greater incidence of CEUs in soleus from dCASQ-null mice correlated with increased specific force production during repetitive, high-frequency stimulation, which depended on Ca^{2+} entry. Consistent with this, Orai1 expression was significantly increased in soleus of CASQ1-null mice, but even more in dCASQ-null mice, compared with WT. Together, these results strengthen the concept that CEU assembly strongly depends on CASQ expression and provides an alternative source of Ca^{2+} needed to refill SR Ca^{2+} stores to maintain specific force production during sustained muscle activity.

Introduction

Calcium (Ca^{2+}) is a universal second messenger that controls a large number of cellular functions in virtually all cells. Therefore, cellular levels of Ca^{2+} need to be precisely regulated. In skeletal muscle fibers, Ca^{2+} plays the crucial role in determining contraction and relaxation. Muscle contraction occurs when free cytoplasmic Ca^{2+}, kept at very low levels (~10^{-7} M) under resting conditions, rises upon Ca^{2+} release from the SR, the primary intracellular Ca^{2+} store. The rapid increase of cytosolic Ca^{2+} needed for contraction is finely controlled by a highly organized sarcotubular membrane apparatus termed the triad or Ca^{2+} release unit (Franzini-Armstrong and Jorgensen, 1994). The triad, composed of a central transverse tubule (T-tubule), a specialized invagination of the sarcolemma, and two adjacent SR terminal cisternae or junctional SR (jSR), is the site of excitation–contraction (EC) coupling. EC coupling is the mechanism whereby an action potential propagating down the T-tubule membrane triggers the release of Ca^{2+} from the SR terminal cisternae as a result of a mechanical interaction between two proteins: (1) the dihydropyridine receptor voltage sensor (DHPR or Cav1.1) in the T-tubule and (2) type 1 ryanodine receptor (RyR1) Ca^{2+} release channel in the SR (Schneider and Chandler, 1973; Ríos et al., 1992; Ríos et al., 1993; Schneider, 1994). Electron microscopy (EM) images show that the small junctional gap (~12 nm) that separates the jSR and T-tubule membranes that form the triad is filled by small electron densities, called "feet," which represent the large RyR1 cytoplasmic

[1]Center for Advanced Studies and Technology, University G. d'Annunzio of Chieti-Pescara, Chieti, Italy; [2]Department of Chemistry, Biology, and Biotechnology, University of Perugia, Perugia, Italy; [3]Department of Medicine and Aging Sciences, University G. d'Annunzio of Chieti-Pescara, Chieti, Italy; [4]Department of Pharmacology and Physiology, School of Medicine and Dentistry, University of Rochester, Rochester, NY; [5]Department of Neuroscience, Imaging, and Clinical Sciences, University G. D'Annunzio of Chieti-Pescara, Chieti, Italy.

Correspondence to Simona Boncompagni: simona.boncompagni@unich.it; Antonio Michelucci: antonio.michelucci@unipg.it

This work is part of a special issue on excitation–contraction coupling.

domains (Franzini-Armstrong, 1970; Franzini-Armstrong et al., 1999).

To release a sufficient amount of Ca^{2+} needed to drive contraction, the lumen of the jSR contains calsequestrin (CASQ), a high-capacity, low-affinity, Ca^{2+} binding protein that increases the SR capacity to store Ca^{2+} (each CASQ molecule binds ≤60–80 Ca^{2+} ions; Cozens and Reithmeier, 1984; Ikemoto et al., 1972; MacLennan and Wong, 1971), while maintaining a relatively low free Ca^{2+} concentration (~400–500 µM) within the SR lumen (Canato et al., 2010; Ziman et al., 2010; Sztretye et al., 2011). As a result, a large accessible pool of Ca^{2+} is present at sites of Ca^{2+} release during EC coupling. Following contraction, myoplasmic Ca^{2+} reuptake is mediated by sarco/endoplasmic reticulum Ca^{2+} ATPase (SERCA) pumps, abundantly present in the longitudinal or "free" SR, during muscle relaxation. CASQ exists in two isoforms known as CASQ1 (or skeletal) and CASQ2 (or cardiac). In slow-twitch (type I) muscle fibers exhibiting a highly oxidative metabolism, both CASQ1 and 2 are expressed, although CASQ1 is the predominant isoform (with a ratio of ~3:1; Fliegel et al., 1989; Damiani et al., 1990; Biral et al., 1992; Sacchetto et al., 1993; Murphy et al., 2009). In contrast, fast-twitch (type IIX/IIB) fibers, primarily characterized by glycolytic metabolism, express only CASQ1, with a total amount greater than that of slow-twitch fibers (Sacchetto et al., 1993; Leberer and Pette, 1986; Leberer et al., 1988). Intermediate-twitch fibers (IIA), which use both aerobic and anaerobic energy systems and fatigue more slowly than type IIX/IIB fibers, are thought to express only CASQ1. However, to date, definitive data are not available regarding the expression of the two different CASQ isoforms in single fibers (Damiani and Margreth, 1994; Froemming et al., 2000). Interestingly, mice deficient for CASQ1 (CASQ1-null) are viable, although fast-twitch fibers exhibit a marked decrease of both jSR cisternae volume and luminal Ca^{2+} buffering, which results in severe SR Ca^{2+} depletion during repetitive stimulation (Paolini et al., 2007; Canato et al., 2010).

As the result of a high level of SERCA expression in skeletal muscle, SR Ca^{2+} reuptake is extremely efficient following Ca^{2+} release during EC coupling. Indeed, it has long been believed that influx of external Ca^{2+} had no role in skeletal muscle contraction (Armstrong et al., 1972). However, over the past two decades, store-operated Ca^{2+} entry (SOCE), the main Ca^{2+} influx pathway triggered by Ca^{2+} store depletion in non-excitable cells (Putney, 1986; Parekh and Putney, 2005), was shown to play a key role in maintaining muscle contractility during repetitive, high-frequency stimulation (Kurebayashi and Ogawa, 2001; Wei-Lapierre et al., 2013; Boncompagni et al., 2017; Michelucci et al., 2018; Michelucci et al., 2019; Michelucci et al., 2020). Similar to non-excitable cells, SOCE in skeletal muscle is also mediated by a functional mechanical coupling between STIM1, the SR Ca^{2+} sensor, and Orai1, a Ca^{2+} permeable channel in the T-tubule (Lyfenko and Dirksen, 2008; Stiber et al., 2008). While a relatively slow process in non-excitable cells, SOCE activation is significantly faster in skeletal muscle (Launikonis and Ríos, 2007). In this context, a phasic mode of rapidly-activating SOCE (pSOCE) is recruited during single muscle twitches in synchrony with EC coupling in skeletal muscle fibers (Koenig et al., 2018; Koenig et al., 2019).

For SOCE to occur, there is a strict requirement of close apposition between the surface and Ca^{2+} store membranes. We recently reported the presence of junctions between stacks of SR cisternae and extension of the T-tubule within the I band of the sarcomere distinct from triads, in fast-twitch muscle (both extensor digitorum longus [EDL] and flexor digitorum brevis [FDB]). While the incidence of these junctions within the I band is very low under resting conditions (sedentary mice) in WT mice, their incidence is significantly increased following acute treadmill exercise. Moreover, the exercise-induced increase in the incidence of these junctions correlates with increased STIM1/Orai1 colocalization, SOCE activity, and maintenance of SR Ca^{2+} release and force production during repetitive, high-frequency stimulation (Boncompagni et al., 2017; Boncompagni et al., 2018; Michelucci et al., 2019). Assembly of these T-tubule/SR stack junctions within the I band of fast-twitch muscle, referred to as Ca^{2+} entry units (CEUs; Boncompagni et al., 2017), is dynamic, as they increase during acute exercise and then progressively disassemble following a subsequent prolonged period of inactivity (≥6 h; Michelucci et al., 2019). On the other hand, CASQ1 deficiency results in constitutive (or stable) assembly of a high incidence of CEUs, which enhances both constitutive and maximum SOCE to counteract the loss of an important Ca^{2+}-bound pool within the SR lumen (Michelucci et al., 2020). However, the presence and functional role of CEUs, as well as their dependence on CASQ, in slow-twitch muscle is completely unknown.

Considering previously reported results observed in both fast-twitch EDL and FDB muscles (Michelucci et al., 2020), herein we set out to characterize the impact of CASQ on CEUs and muscle fatigue in "slow" twitch soleus muscle. Since slow-twitch type I fibers, which represent ~40% of the total in soleus muscle, express both CASQ1 and CASQ2, we analyzed the ultrastructure and function of soleus muscles from WT mice (as control) and mice that lack only CASQ1 (CASQ1-null) or both CASQ1 and CASQ2 (dCASQ-null). These models enabled assessment of the impact of both partial (CASQ1-null) and total (dCASQ-null) CASQ deficiency, as well as the potential for differential contribution of the two isoforms in CEU formation and fatigue. Where appropriate, parallel experiments in EDL muscle were either repeated or reproduced from previous publications for comparison.

Materials and methods

Animals

4–6-mo-old male WT, CASQ1-null, and dCASQ-null mice on congenic C57BL/6 background were housed in microisolator cages at 20°C in a 12-h light/dark cycle while being provided free access to standard food and water. All animal studies were designed to minimize animal suffering and approved by the Animal Ethical Committees at the University of Chieti and the University of Rochester (UCAR-2006-114E).

EM

Intact soleus and EDL muscles were fixed at room temperature with 3.5 or 6% glutaraldehyde in 0.1 M sodium cacodylate buffer

(pH 7.2) and processed for EM acquisition as previously described (Michelucci et al., 2019). For T-tubule staining, muscle samples were postfixed in a mixture of 2% OsO_4 and 0.8% potassium ferrocyanide for 1–2 h followed by rinse with 0.1 M NaCaCo buffer with 75 mM $CaCl_2$. Potassium ferrocyanide precipitate within the T-tubule network is visualized as an electron-dense dark precipitate in EM images (Boncompagni et al., 2017). Ultrathin sections (~50 nm) were cut using a Leica Ultracut R microtome (Leica Microsystem) with a diamond knife (Diatome) and double-stained with uranyl acetate and lead citrate. Sections were viewed in a FP 505 Morgagni Series 268D electron microscope (FEI Company), equipped with Megaview III digital camera and Soft Imaging System at 60 or 100 kV (for T-tubule staining preparations).

Quantitative analyses of EM images

The incidence of both SR stacks and T-tubule/SR stack junctions (i.e., CEUs; 100 μm²) were determined from electron micrographs of nonoverlapping regions randomly collected from transversal EM sections by counting the number of stacks or CEUs per area of section (100 μm²) as described previously (Boncompagni et al., 2017; Michelucci et al., 2019). For each specimen, 10–15 representative fibers were analyzed, and 5 micrographs at 28,000× magnification were taken for each fiber. Extensions of the T-tubule network within the I band (recognizable in cross sections by the presence of the Z-line; Fig. 2 A) of the sarcomere (total T-tubule length) and T-tubule/SR stack contact length (i.e., length of the association between T-tubule and SR stack membranes) were measured in electron micrographs of nonoverlapping regions randomly collected from transversal EM sections in which T-tubules were clearly visible when stained in black with potassium ferrocyanide (Fig. 2 A). For each specimen, 10–15 representative fibers were analyzed, and 5 micrographs at 28,000× magnification were taken for each fiber. Quantitative analyses of SR stacks and T-tubule network extension were obtained using Analy-SIS software of the EM digital camera (Olympus Soft Imaging Solutions). Specifically, the quantitative parameters "number of SR stacks" and "total T-tubule length" at I band were obtained through a computer-assisted morphometric analysis of EM images recorded from each section of random, but nonoverlapping, fields as follows: (1) number of SR stacks was obtained by counting in each EM image at 28,000× magnification (covering an area of 8.9 μm²) the number of flat parallel SR cisternae, reported as number/area of section (100 μm²); (2) total T-tubule length at I band was measured in each EM image using the polygon length tool of the Analysis software of the electron microscope, which allows complete geometric measurements of structures, such as T-tubules, by drawing their outline. The outline of T-tubules at the I band was measured in each EM image at 28,000× magnification (covering an area of 8.9 μm²), reported as number/area of section (100 μm²).

EM fiber type analysis in soleus muscle

The soleus is composed mainly of two types of fibers: type I (~40% of the total) and type IIA (~60% of the total). Ultrastructurally, type I and IIA can be distinguished from each other on the basis of Z-line width (~70 nm in IIA and ~90 nm in type I; Boncompagni et al., 2010) in longitudinal sections. However, the classification of individual images in the two categories of fiber types is not reliably achieved owing to some native variation of the Z-line width and because the apparent Z-line width in the image is affected by section orientation. For this reason, and because the ultrastructural data we analyzed (i.e., incidence of CEUs, T-tubule length, and SR/T-tubule contact length) did not exhibit a bimodal distribution as would be expected if there were significant differences between type I and IIA fibers, all data were combined in the analyses.

Ex vivo contractility

Ex vivo assessment of muscle force production was conducted in intact soleus and EDL muscles excised from WT, CASQ1-null, and dCASQ-null mice. Excised muscles were attached to a servo motor and force transducer (1200 A; Aurora Scientific) placed between two platinum electrode plates in a chamber continuously perfused with oxygenated Ringer solution as previously described (Michelucci et al., 2019). For both soleus and EDL muscles, optimal stimulation level and muscle length (L_0) were determined using a series of 1-Hz twitch stimulation trains while stretching the muscle to a length that generated maximal force (F_0). After establishing L_0, muscles were first equilibrated using three tetani (500 ms, 150 Hz) given at 1-min intervals. After 5 min of rest, muscles were then subjected to a repetitive stimulation protocol: for soleus muscles (60 consecutive, 1-s-duration, 50-Hz-stimulus trains delivered every 2.5 s, duty cycle 0.4); for EDL muscles (60 consecutive, 500-ms-duration, 50-Hz-stimulus trains delivered every 2.5 s, duty cycle 0.2). All muscle contractility experiments were carried out at 30°C. Muscle force was recorded using Dynamic Muscle Control software and analyzed using a combination of both Dynamic Muscle Analysis (Aurora Scientific) and Clampfit 10.0 (Molecular Devices) software. Specific force was calculated by normalizing the absolute force to the physiological cross sectional area as previously described (Michelucci et al., 2019; Michelucci et al., 2020).

Western blot

Soleus and EDL muscles were dissected, snap frozen in liquid nitrogen, and homogenized in radioimmunoprecipitation assay lysis buffer (RIPA; 20 mM Tris-HCl, 150 mM NaCl, 1 mM Na_2EDTA, 1 mM EGTA, 1% NP-40, 1% sodium deoxycholate, 2.5 mM sodium pyrophosphate, 1 mM *b*-glycerophosphate, 1 mM Na_3VO_4, and 1 μg/ml leupeptin, pH 7.5) supplemented with a cocktail of protease inhibitors. Protein concentration was determined spectrophotometrically using both Lowry and bicinchoninic acid assays. Briefly, 10–20 μg of total protein was resolved in 10% polyacrylamide electrophoresis gels, transferred to nitrocellulose membrane, and blocked with 5% nonfat dry milk (Bio-Rad) in Tris-buffered saline 0.1% and Tween 20 (TBS-T) for 1–1.5 h. Membranes were probed with the following primary antibodies diluted in 5% nonfat dry milk in TBS-T overnight at 4°C: STIM1 antibody (rabbit polyclonal diluted 1:2,500; Sigma Aldrich); Orai1 (mouse monoclonal diluted 1:1,000; Santa Cruz Biotechnology); and GAPDH (mouse monoclonal diluted 1:10,000; Invitrogen), used as loading control. Membranes

were washed three times in TBS-T and incubated with goat anti-mouse IgG-800 and goat anti-rabbit IgG-800 (diluted 1:10,000; Invitrogen) secondary antibodies diluted in 5% nonfat dry milk in TBS-T for 1 h at room temperature. Proteins were visualized on an Odyssey Infra-red imager (Li-Cor). Quantitative analyses of protein expression was performed on exported .TIFF images using ImageJ software (National Institutes of Health).

Isolation of FDB muscle fibers

FDB muscle fibers were dissected from hind paws of 4–6-mo-old mice and placed in a dish containing Ringer's solution consisting of 145 mM NaCl, 5 mM KCl, 2 mM $CaCl_2$, 1 mM $MgCl_2$, and 10 mM HEPES, pH 7.4. Muscle fibers were enzymatically dissociated by incubating FDB muscles in Ringer's solution supplemented with 1 mg/ml collagenase A (Roche) for 60 min while rocking gently at 37°C. Single fibers were then obtained by mechanical dissociation/trituration, plated on glass-bottom dishes, and allowed to settle for >20 min before conducting Mn^{2+} quench experiments (see next section). Only fibers with a clean morphology, clear striations, and no signs of swelling or damage were used for recordings.

Mn^{2+} quench of fura-2 fluorescence

For measurements of Mn^{2+} quench of fura-2 fluorescence, FDB fibers were loaded with 5 µM fura-2 AM for 1 h at 37°C in a Ca^{2+}-free Ringer's solution containing 145 mM NaCl, 5 mM KCl, 3 mM $MgCl_2$, and 0.2 EGTA, pH 7.4. To deplete SR Ca^{2+} stores before measurements of Mn^{2+} quench, fibers were also exposed to two SERCA pump inhibitors (1 µM thapsigargin; 15 µM cyclopiazonic acid) during the fura-2 loading period (+depletion). A skeletal muscle myosin inhibitor (30 µM *N*-benzyl-*p*-toluene sulfonamide) was also included in all isolated fiber solutions to prevent movement artifacts (Wei-Lapierre et al., 2013). In a second set of studies, FDB fibers were loaded with fura-2 AM and *N*-benzyl-*p*-toluene sulfonamide in the absence of SERCA pump inhibitors (–depletion). Both store-depleted and nondepleted FDB fibers were then bathed in Ca^{2+}-free Ringer's and excited at 362 nm (isobestic point of fura-2), while emission was detected at 510 nm using a DeltaRam illumination system (Photon Technology). After obtaining an initial basal rate of fura-2 decay ($R_{baseline}$), fibers were exposed to Ca^{2+}-free Ringer's supplemented with 0.5 mM $MnCl_2$. The maximum rate of fura-2 quench in the presence of Mn^{2+} (R_{max}) was calculated from the peak time derivative of the fura-2 emission trace during Mn^{2+} application. The maximum rate of SOCE (R_{SOCE}) was calculated as $R_{SOCE} = R_{max} - R_{baseline}$ and expressed as dF/dt in counts/s (Wei-Lapierre et al., 2013).

Statistical analyses

Statistical significance was determined using a one-way ANOVA followed by post hoc Tukey test for multiple comparisons. Amplitude histograms of maximal rates of Mn^{2+} quench were fitted according to a single Gaussian distribution. In all cases, differences were considered statistically significant at $P < 0.05$ (P values are provided in figure legends). All data are presented as mean ± SEM.

Online supplemental material

Fig. S1 shows the comparison of the incidence of SR stacks and CEUs, T-tubule extensions, and T-tubule/SR stack contact length between EDL and soleus muscle fibers, assessed by EM quantitative analysis. Fig. S2 summarizes the specific force during repetitive high-frequency stimulation of intact EDL muscles in the presence or absence of extracellular Ca^{2+} influx, in ex vivo contractile experiments. Fig. S3 shows Western blot analyses of proteins that coordinate SOCE (i.e., STIM1 and Orai1) in EDL muscle homogenates. Fig. S4 presents the maximum rate of Mn^{2+} quench in FDB fibers in the presence or absence of pharmacological SR Ca^{2+} store depletion.

Results

Increased incidence of preassembled SR/T-tubule junctions within the I band of the sarcomere in soleus muscle from both CASQ1-null and dCASQ-null mice

We previously reported that the absence of CASQ1 promoted the constitutive assembly of T-tubule/SR stack junctions within the I band of the sarcomere in fast-twitch fibers of EDL muscles (Michelucci et al., 2020). These T-tubule/SR stacks junctions were similar to the CEUs described in EDL muscles from WT mice subjected to acute exercise on the treadmill, which contained colocalized STIM1/Orai1 and promoted enhanced constitutive and maximum SOCE (Boncompagni et al., 2017; Boncompagni et al., 2018; Michelucci et al., 2019). However, neither the impact of CASQ1 deficiency nor that of CASQ2 deficiency on the T-tubule/SR remodeling and association within the I band in slow-twitch fibers is known. Using EM analysis, we investigated whether T-tubule/SR stacks junctions also assemble in slow-twitch fibers of soleus muscle. To this aim, we analyzed the ultrastructure of soleus muscles from WT mice and compared them with soleus muscles from CASQ1-null (which lack CASQ1) and dCASQ-null (which lack both CASQ1 and CASQ2 isoforms) mice. As shown in Fig. 1, we stained soleus muscles with ferrocyanide, which forms a dark precipitate that enables direct visualization of T-tubule membranes. Similar to results in EDL and FDB fibers from CASQ1-null mice (Michelucci et al., 2020), we found that longitudinal T-tubule membranes were significantly more abundant in soleus muscle fibers from both CASQ1-null and dCASQ-null mice compared with WT mice (Fig. 1, A–D). Importantly, we also noted that the longitudinal T-tubules within the I band were often associated with flat SR cisternae elements (Fig. 1, E–H), resulting in the assembly of junctions similar to CEUs described previously in fast twitch muscle (Boncompagni et al., 2017; Michelucci et al., 2019). Morphologically, the only difference between these junctions and CEUs in fast-twitch muscle is that elongated T-tubules in soleus muscle from both CASQ1-null and dCASQ-null mice typically associate with only one SR cisternae element (Fig. 1, E and G), although association with two SR elements is occasionally observed (Fig. 1, F and H). T-tubule association with stacks of more of two SR elements, frequently observed in fast-twitch muscle fibers, were not found in soleus muscle.

CEUs in fast-twitch muscle fibers are composed of T-tubule extensions (which contain Orai1) in association with SR stacks

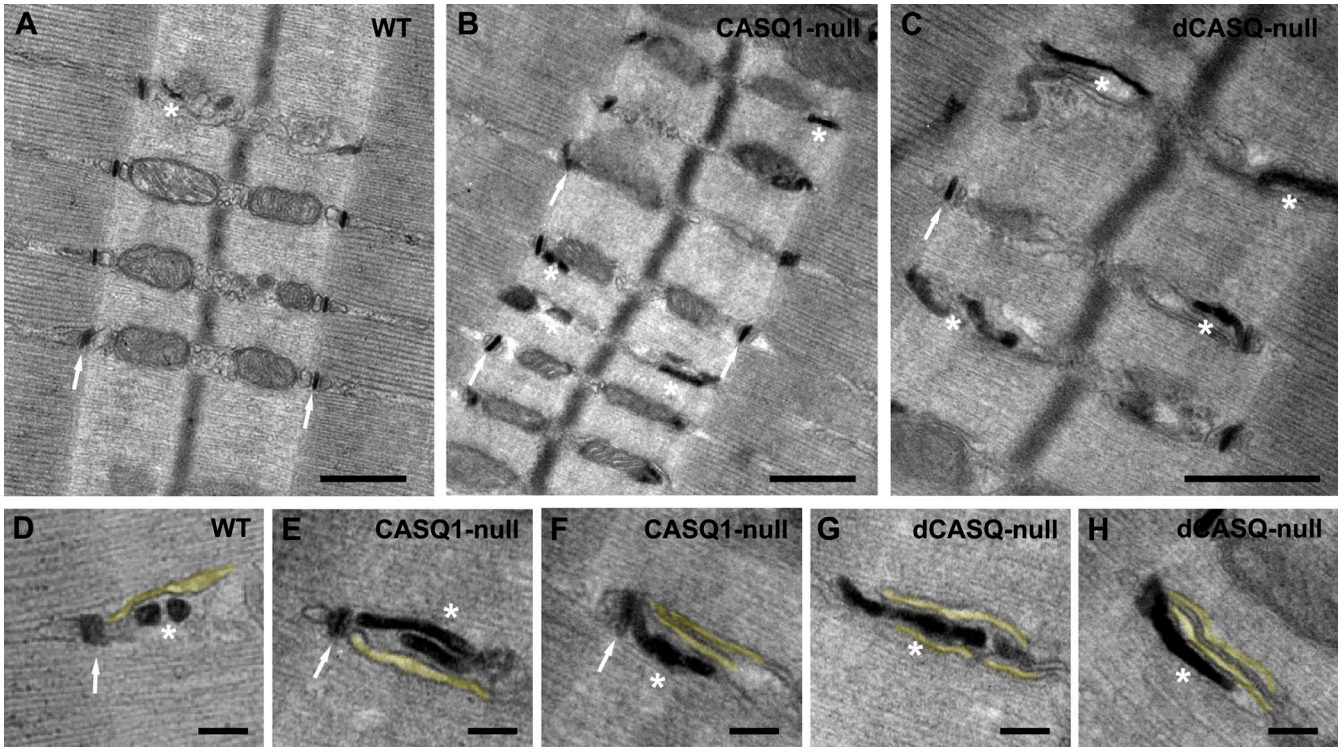

Figure 1. **Qualitative evaluation of T-tubule/SR junctions (i.e., CEUs) within the I band of solues muscle fibers. (A–H)** Representative EM images in longitudinal sections of soleus fibers from WT (A and D), CASQ1-null (B, E, and F), and dCASQ-null (C, G, and H) mice at 4 mo of age in which T-tubules are stained in black with ferrocyanide. White arrows point to longitudinal triadic T-tubules, whereas white asterisks point to transversal T-tubule extensions at the I band. **(D–H)** SR membrane forming flat cisternae at the I band are false labeled in yellow. White numbers mark each SR cisternae element. Scale bars: A–C, 0.5 µm; D–H, 0.1 µm.

(that contain STIM1) within the I band (Boncompagni et al., 2017; Michelucci et al., 2019; Michelucci et al., 2020). To confirm the similar visual observation of CEUs in slow-twitch muscle as shown in Fig. 1, we quantified (1) the incidence of SR stacks constituted by at least two SR elements; (2) the total T-tubule length at the I band; (3) the incidence of T-tubule/SR stack junctions (i.e., CEUs), and (4) the extent of T-tubule contact with SR cisternae elements (T-tubule/SR stack contact length). All parameters were evaluated in EM cross sections of soleus muscle fibers postfixed in the presence of ferrocyanide (Fig. 2 A). Quantitative analysis revealed that the number of SR stacks constituted by at least two elements were very low in muscle fibers from WT mice (0.49 ± 0.6/100 µm^2), and not statistically higher in CASQ1-null mice (0.75 ± 0.3/100 µm^2), but statistically more abundant in dCASQ-null mice (1.2 ± 0.2/100 µm^2; Fig. 2 B). On the other hand, total T-tubule length at the I band in soleus fibers from CASQ1-null (8.9 ± 0.5/100 µm^2) and dCASQ-null (9.1 ± 0.6/100 µm^2) mice (Fig. 2 C) was approximately five times higher than that observed in fibers of WT mice (1.8 ± 0.2/100 µm^2), with dCASQ1-null mice showing a T-tubule length statistically higher than that of CASQ1-null mice. Consistent with this increased T-tubule length at the I band in soleus muscle from both CASQ knockout (KO) mice, the incidence of T-tubule association with a SR cisternae element within the I band was increased, and in fact, very similar to that observed for CEUs in EDL muscle fibers (Boncompagni et al, 2017; Michelucci et al, 2020). The quantitative analysis also revealed that the number of T-tubule/SR stack junctions (i.e., CEUs) per area of cross section was 16.2 ± 1.1 and 18.4 ± 1.3/100 µm^2 in CASQ1-null and dCASQ-null mice, respectively, versus only 4.9 ± 0.5/100 µm^2 in WT mice (Fig. 2 D). In addition, the length of T-tubule contact with SR cisternae elements was ∼10 and 15 times greater in CASQ1-null (1.9 ± 0.3/100 µm^2) and dCASQ-null (3.0 ± 0.5/100 µm^2) mice, respectively, compared with WT mice (0.2 ± 0.07/100 µm^2; Fig. 2 E). Similarly, EDL muscles from both CASQ1-null and dCASQ-null mice exhibited increased higher incidence of SR stacks, T-tubule length, incidence of CEUs, and T-tubule/SR stack association compared with WT mice, although no difference were observed in EDL muscle between the two KO genotypes (Fig. S1; Michelucci et al., 2020). Note that longitudinal triads, frequently present in CASQ-null mice, are morphologically different and easily recognizable from CEUs (Fig. 2 A, top and middle small panels on the right) in EM cross sections.

Increased peak specific force during repetitive stimulation in soleus and EDL muscles from CASQ1-null and dCASQ-null mice depends on extracellular Ca^{2+} entry

The results obtained from the quantitative ultrastructural EM studies indicated that CASQ deficiency in soleus muscle coincides with a significant increase in the incidence of T-tubule/SR stack junctions within the I band of the sarcomere that closely resemble CEUs in EDL muscle (Boncompagni et al., 2017; Michelucci et al., 2019; Michelucci et al., 2020). Increases in

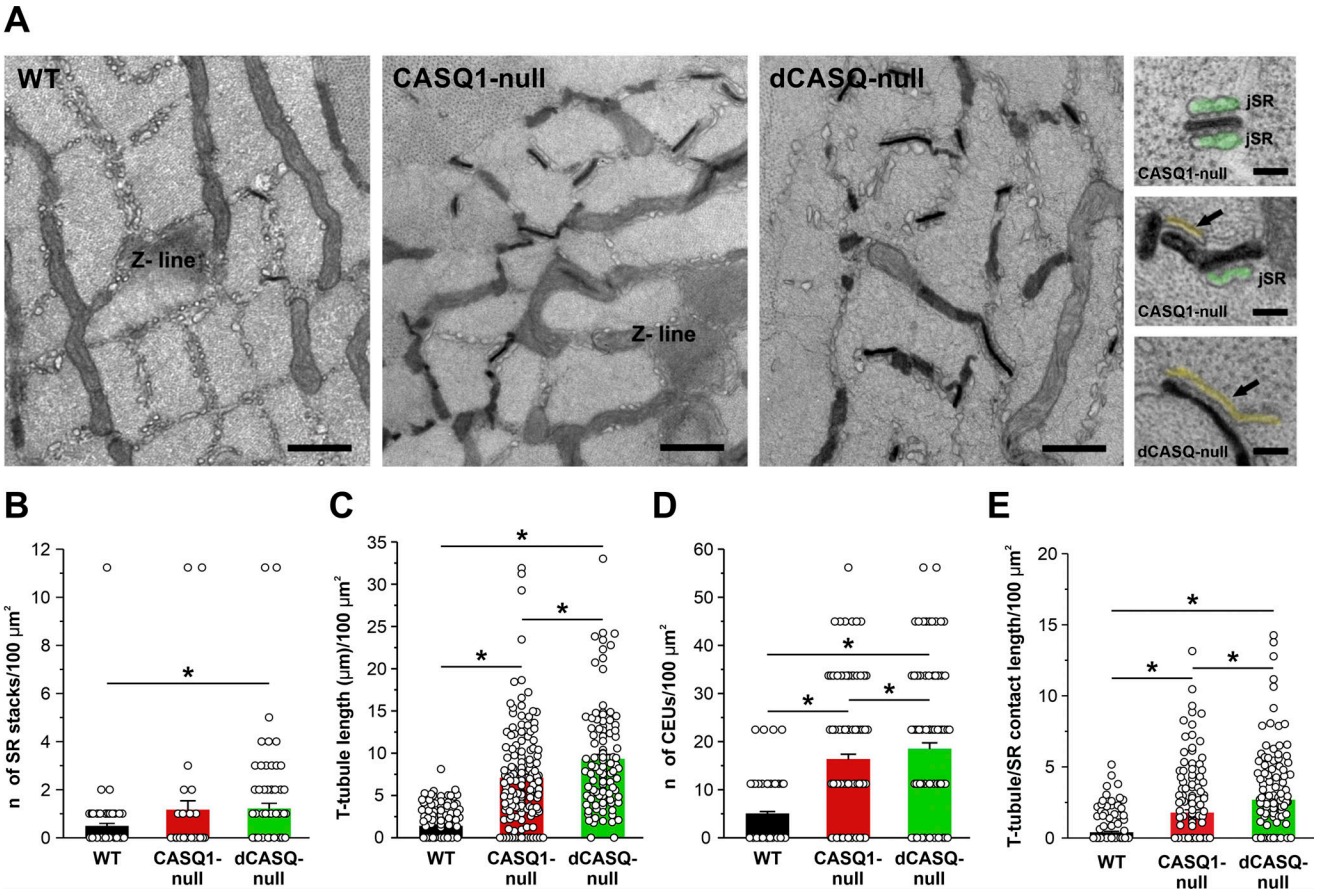

Figure 2. **Incidence of SR stacks and CEUs, T-tubule extensions, and T-tubule/SR stack contact length in soleus muscle fibers. (A)** Representative EM images of cross sections of soleus muscle fibers from WT (left), CASQ1-null (middle), and dCASQ-null (right) mice and higher-magnification EM images (vertical panels) showing T-tubules stained in black with ferrocyanide precipitate. Color labeling: jSR, false labeled in green; SR cisternae element of a CEU, false labeled in yellow and pointed to by black arrows. Scale bars: horizontal panels (left), 1 µm; vertical panels (right) 0.1 µm. **(B–E)** Bar plots showing quantitative analyses of the number of SR stacks (B), T-tubule length (C), the number of CEUs (D), and T-tubule/SR stack contact length (E) in the I band (expressed as µm/100 µm² of cross-sectional area) in soleus muscle fibers from WT (n = 109; n = 158; n = 158; n = 158 fibers), CASQ1-null (n = 32; n = 148; n = 148; n = 148 fibers), and dCASQ-null (n = 84; n = 125; n = 109; n = 125 fibers) mice. Data are shown as mean ± SEM. Statistical significance: B: *, P = 0.015, WT vs. dCASQ-null; C: *, P = 0.00000004, WT vs. CASQ1-null; *, P = 0.00000003, WT vs. dCASQ-null; D: *, P = 0.00000004, WT vs. CASQ1-null; *, P = 0.00000002, WT vs. dCASQ-null; *, P = 0.00082, CASQ1-null vs. dCASQ-null. Number of mice used: WT, n = 3; CASQ1-null, n = 3; dCASQ-null, n = 3.

CEUs correlate with both enhanced constitutive Ca^{2+} entry and SOCE, as well as sustained Ca^{2+} release and muscle specific force production during repetitive stimulation (Boncompagni et al., 2017; Michelucci et al., 2019; Michelucci et al., 2020); therefore we evaluated the ability of intact soleus muscles from WT, CASQ1-null, and dCASQ-null mice to maintain contractile force when subjected to a repetitive, high-frequency stimulation protocol. We assessed specific force in standard Ringer solution (containing 2.5 mM Ca^{2+}), as well as under conditions designed to reduce/abolish Ca^{2+} entry (i.e., 0 Ca^{2+} and 10 µM BTP2; Fig. 3). In the presence of extracellular Ca^{2+}, peak specific force of the first stimulus train was not significantly different between WT and CASQ1-null mice, while a significant reduction in force was observed in soleus muscles from dCASQ-null mice (Fig. 3 A). However, the time course of peak specific force decline during the protocol differed markedly between the three genotypes. In fact, while a constant gradual reduction of specific force was observed during the protocol in WT mice, soleus muscles from both CASQ1-null and dCASQ-null mice exhibited a pronounced drop in specific force during the second to fourth stimulus trains, followed by a marked rebound increase (Fig. 3 A). Interestingly, both the initial force drop and rebound increase were significantly more pronounced in dCASQ-null muscles compared with CASQ1-null mice. Specifically, both the reduction in specific force during the fourth stimulus (ratio between specific force produced during the fourth and first stimuli [ST_{4th}/ST_{1st}]) and rebound increase (ratio between peak specific force produced during the peak and fourth stimuli [ST_{peak}/ST_{4th}]) were virtually absent in soleus muscles from WT mice (−0.07 ± 0.005 and 0.8 ± 0.03), larger in CASQ1-null mice (−0.13 ± 0.008 and 1.05 ± 0.01), and highest in dCASQ-null mice (−0.26 ± 0.03 and 1.4 ± 0.09; Fig. 3 B). As previously reported in EDL muscle, the pronounced force drop decay following the first stimulus reflects a combination of (1) high SR "Ca^{2+} evacuability" (Royer et al., 2010), (2) significant reduction in total releasable Ca^{2+} store content (Lamboley et al., 2015; Michelucci et al., 2020), and (3) decrease in luminal free Ca^{2+} concentration during electrical stimulation (Michelucci et al., 2020). On the

other hand, the rebound increase in peak force production observed with CASQ deficiency is a reflection of increased SOCE activity (Michelucci et al., 2019; Michelucci et al., 2020). These findings suggested that Ca^{2+} influx via SOCE was increased during repetitive stimulation in soleus muscles from CASQ1-null mice, and even more in dCASQ-null mice, which would counteract the massive SR depletion from CASQ deficiency. To confirm the contribution of Ca^{2+} influx during the rebound increase in specific force observed in CASQ1-null and dCASQ-null mice, identical measurements were performed under experimental conditions designed to limit/block Ca^{2+} entry, including perfusion in (1) nominally Ca^{2+}-free Ringer solution (equimolar replacement with Mg^{2+}; Fig. 3, B and E) and (2) standard Ringer supplemented with 10 µM BTP2, a potent SOCE inhibitor (Zitt et al., 2004). In line with previous studies conducted in EDL muscles (Boncompagni et al., 2017; Michelucci et al., 2019; Michelucci et al., 2020), the rebound increase in specific force production observed in soleus muscles from CASQ1-null and dCASQ-null mice was absent under conditions where Ca^{2+} entry was abolished (Fig. 3, C–F). Similarly, EDL muscles from both CASQ1-null and dCASQ-null mice exhibited an increased ability to maintain specific force during repetitive, high-frequency stimulation in the presence of extracellular Ca^{2+}. Consistent with previous results (Michelucci et al., 2019; Michelucci et al., 2020), this rebound increase in specific force production was abolished when Ca^{2+} entry was prevented by removing external Ca^{2+} or adding 10 µM BTP2 (Fig. S2). However, unlike soleus muscle, no differences were observed in EDL muscle between the two CASQ KO genotypes (Fig. S2).

Increased Orai1 expression in soleus muscles of both CASQ1-null and dCASQ-null mice

Given the increased ability of soleus muscles in CASQ1-null and dCASQ-null mice to maintain force production during repetitive stimulation, which was abolished when Ca^{2+} influx was prevented, we quantified the expression of the two key proteins that form the core SOCE machinery in muscle (i.e., STIM1 and Orai1; Fig. 4). Results from these experiments revealed that while the relative expression of both the short (STIM1S) and long (STIM1L) STIM1 splice variants in soleus muscle were not significantly different among the three genotypes (Fig. 4, A and C), expression of Orai1 was two- to threefold higher in soleus muscle homogenates from CASQ1-null and dCASQ-null mice compared with WT mice (Fig. 4, B and D). Interestingly, the expression of Orai1 was significantly higher in soleus muscles from dCASQ-null than CASQ1-null mice. Specificity of the Orai1 antibody was validated by showing the absence of reactivity in soleus muscles from constitutive, muscle-specific Orai1 KO mice (cOrai1 KO), as previously reported (Michelucci et al., 2020). On the other hand, STIM1S, STIM1L, and Orai1 were all increased significantly in EDL muscles from both CASQ1-null and dCASQ-null mice compared with WT mice (Fig. S3). However, in contrast to that observed in soleus muscle (Fig. 4, B and D), Orai1 expression was not statistically different in EDL muscle between the two KO lines (Fig. S3, B and D).

Discussion

Main findings of the study

In the present study, we demonstrate that CEUs assemble in slow-twitch soleus muscle. Similar to previous results (Michelucci et al., 2019; Michelucci et al., 2020), CEU incidence is increased in CASQ-deficient soleus muscle. This increase in CEUs correlates with an enhanced ability to maintain specific force production during repetitive, high-frequency stimulation when Ca^{2+} influx is allowed. In particular, compared with soleus from WT mice, soleus muscle from both CASQ1-null and dCASQ-null mice exhibits a higher incidence of constitutive assembled CEUs (Figs. 1 and 2). However, several important differences are observed with regard to the relative impact of CASQ1 and CASQ2 for CEUs in soleus muscle. While the number of SR stack membranes is not significantly different between CASQ1-null and dCASQ-null mice, longitudinal T-tubule extensions, number of T-tubule/SR stack junctions (i.e., CEUs), and T-tubule/SR stack contact length within the I band are all significantly higher in soleus fibers from dCASQ-null mice (Fig. 2, C–E). Conversely, in EDL muscles, all four parameters were not significantly different between the two CASQ KO mouse lines, although significantly more prevalent than that observed of WT (Fig. S1). One possible explanation for this finding is that the incidence of T-tubule/SR stack junctions (or CEUs) is dictated by relative overall expression level of CASQ proteins. Compared with slow-twitch fibers from soleus muscle from WT mice, T-tubule/SR stack junctions within the I band are more abundant in dCASQ-null than CASQ1-null mice. On the other hand, no difference in CEU incidence is observed in fast-twitch muscle between dCASQ-null and CASQ1-null mice. As we previously found that the dynamic remodeling of T-tubules and their association with SR cisternae elements to form functional CEUs correlates with enhanced Ca^{2+} influx via SOCE in fast-twitch muscle (Michelucci et al., 2019; Michelucci et al., 2020), it is likely that the increase in T-tubule/SR stack junctions observed in CASQ-deficient soleus muscle also enhances SOCE. This notion is corroborated by functional and biochemical experiments showing that soleus muscles from both CASQ1-null and dCASQ-null mice exhibit (1) increased ability to maintain contractile force during repetitive high-frequency stimulation in the presence of extracellular Ca^{2+} (Fig. 3) and (2) increased expression of Orai1 (Fig. 4, B and D). EDL muscles from both CASQ1-null and dCASQ-null mice, which are enriched in CEUs (Michelucci et al., 2020; Fig. S1), also exhibit an increased ability to maintain contraction during repetitive, high-frequency stimulation in the presence of extracellular Ca^{2+} compared with WT mice (Fig. S2). Finally, while expression of Orai1 in soleus muscle is higher in dCASQ-null than CASQ1-null mice (Fig. 4, B and D), no difference was observed in STIM1 between the three groups of mice, while expression of both STIM1 and Orai1 were increased to a similar level compared with WT in EDL muscle of CASQ1-null and dCASQ-null mice (Fig. S3).

Structural, biochemical, and functional differences between soleus muscles from CASQ1-null and dCASQ-null mice

No significant difference was observed in either the incidence of CEUs or contractility properties in EDL muscles from CASQ1-

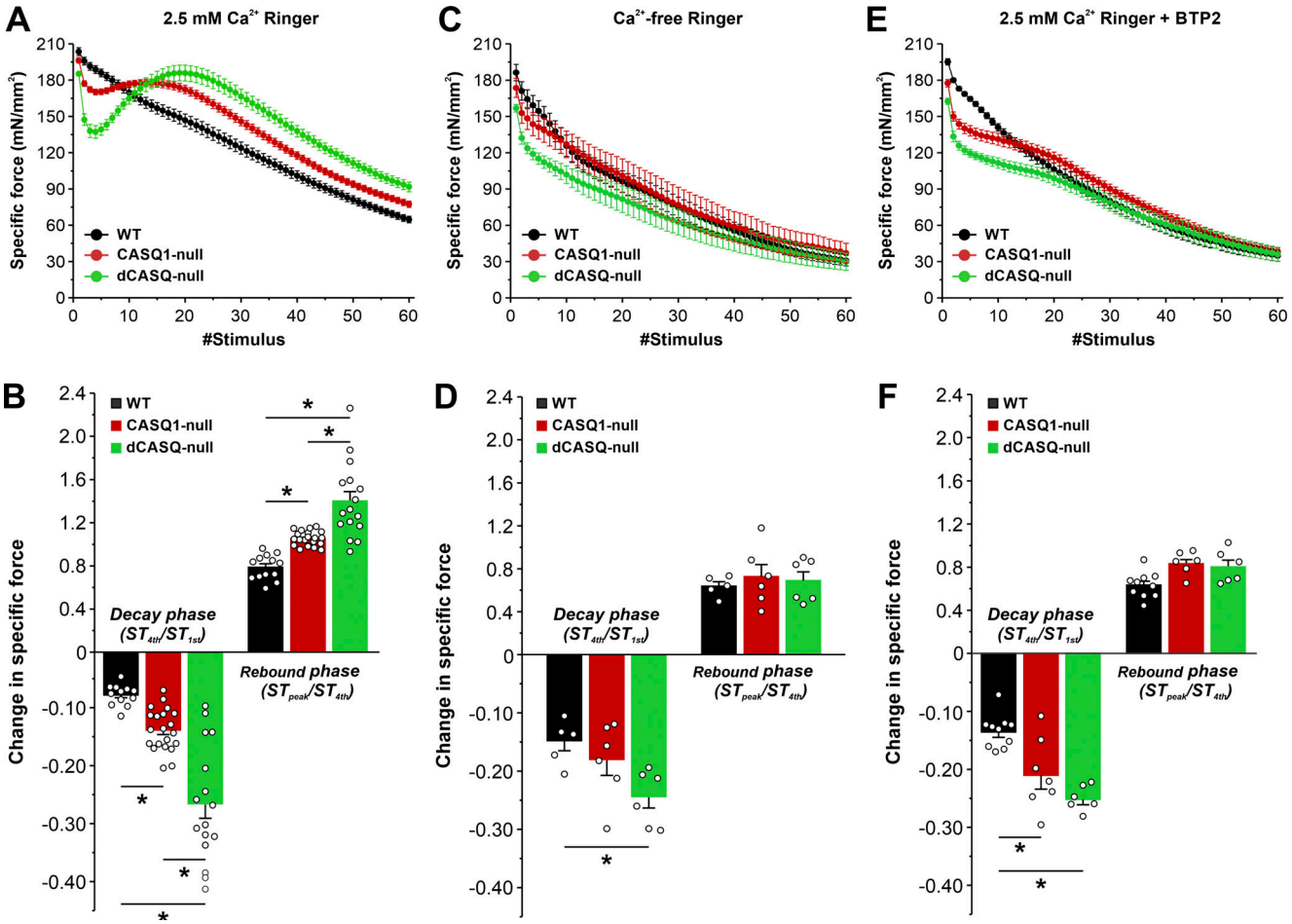

Figure 3. **Ca^{2+} influx dependence of contractile force during repetitive high-frequency stimulation of intact soleus muscles. (A, C, and E)** Time course of peak specific force recorded in soleus muscles from WT (A and B, *n* = 13; C and D, *n* = 5; E and F, *n* = 10 muscles), CASQ1-null (A and B, *n* = 21; C and D, *n* = 6; E and F, *n* = 7 muscles), and dCASQ-null (A and B, *n* = 16; C and D, *n* = 6; E and F, *n* = 6 muscles) mice during 60 consecutive 1-s duration repetitive stimulus trains in the presence of either standard Ringer's solution containing 2.5 mM Ca^{2+} (A), nominally Ca^{2+}-free Ringer's solution (C), or standard Ringer's solution supplemented with 10 µM BTP2 (E). **(B, D, and F)** Quantitative analyses of the relative decay during the fourth stimulus train (ST_{4th}/ST_{1st}) and the peak of the rebound phase (ST_{peak}/ST_{4th}) from the corresponding data shown in A, C, and E. Data are shown as mean ± SEM. Statistical significance: *, P = 0.023, WT vs. CASQ1-null; *, P = 0.00000055, WT vs. dCASQ-null; *, P = 0.00000047, CASQ1-null vs. dCASQ-null; rebound phase: *, P = 0.0026, WT vs. CASQ1-null; *, P = 0.0000025, WT vs. dCASQ-null; *, P = 0.00003, CASQ1-null vs. dCASQ-null. D: decay phase: *, P = 0.027, WT vs. dCASQ-null. F: decay phase: *, P = 0.004, WT vs. CASQ1-null; *, P = 0.00008, WT vs. dCASQ-null. Number of mice used: WT (A and B, *n* = 7; C and D, *n* = 3; E and F, *n* = 7), CASQ1-null (A and B, *n* = 12; C and D, *n* = 4; E and F, *n* = 4); dCASQ-null (A and B, *n* = 12; C and D, *n* = 4; E and F, *n* = 4).

null and dCASQ-null mice. In addition, STIM1 and Orai1 expression in EDL muscles from CASQ1-null and dCASQ-null mice were not statistically different, despite being markedly higher than that observed in WT EDL muscle. On the other hand, marked structural and functional differences were observed between soleus muscles from CASQ1-null and dCASQ-null mice. For example, soleus muscles from dCASQ-null mice exhibited a higher number of CEUs and greater T-tubule/SR stack contact length. These effects correlated well with both a greater rebound increase in specific force production during repetitive simulation and increased expression of Orai1 (dCASQ > CASQ1 > WT). These findings suggest that total CASQ expression in soleus muscle inversely correlates with Ca^{2+} influx via Orai1-dependent SOCE. This idea is consistent with increased SOCE (maximal rate of Mn^{2+} quench of fura-2 fluorescence) observed in FDB fibers from CASQ1-null and dCASQ-null mice (Fig. S4). As a result, the absence of both CASQ isoforms in soleus muscle of dCASQ-null mice results in a greater dependence of muscle contraction on extracellular Ca^{2+}, presumably needed to refill SR Ca^{2+} stores due to a deficit in a robust pool of bound, but exchangeable, Ca^{2+}. This dependence is somewhat less in soleus muscles from CASQ1-null mice, presumably given the higher available Ca^{2+}-bound pool within the SR lumen due to the presence of CASQ2. However, the expression of only CASQ2 in soleus muscles is not sufficient to fully compensate/replace the absence of CASQ1, as demonstrated by the fact that soleus muscles from CASQ1-null mice still exhibit structural (constitutive presence of CEUs), functional (higher decay and rebound contractile phases during repetitive high-frequency stimulation), and biochemical (greater expression of Orai1) alterations compared with WT mice. These results further demonstrate a strong correlation between CASQ expression, incidence of

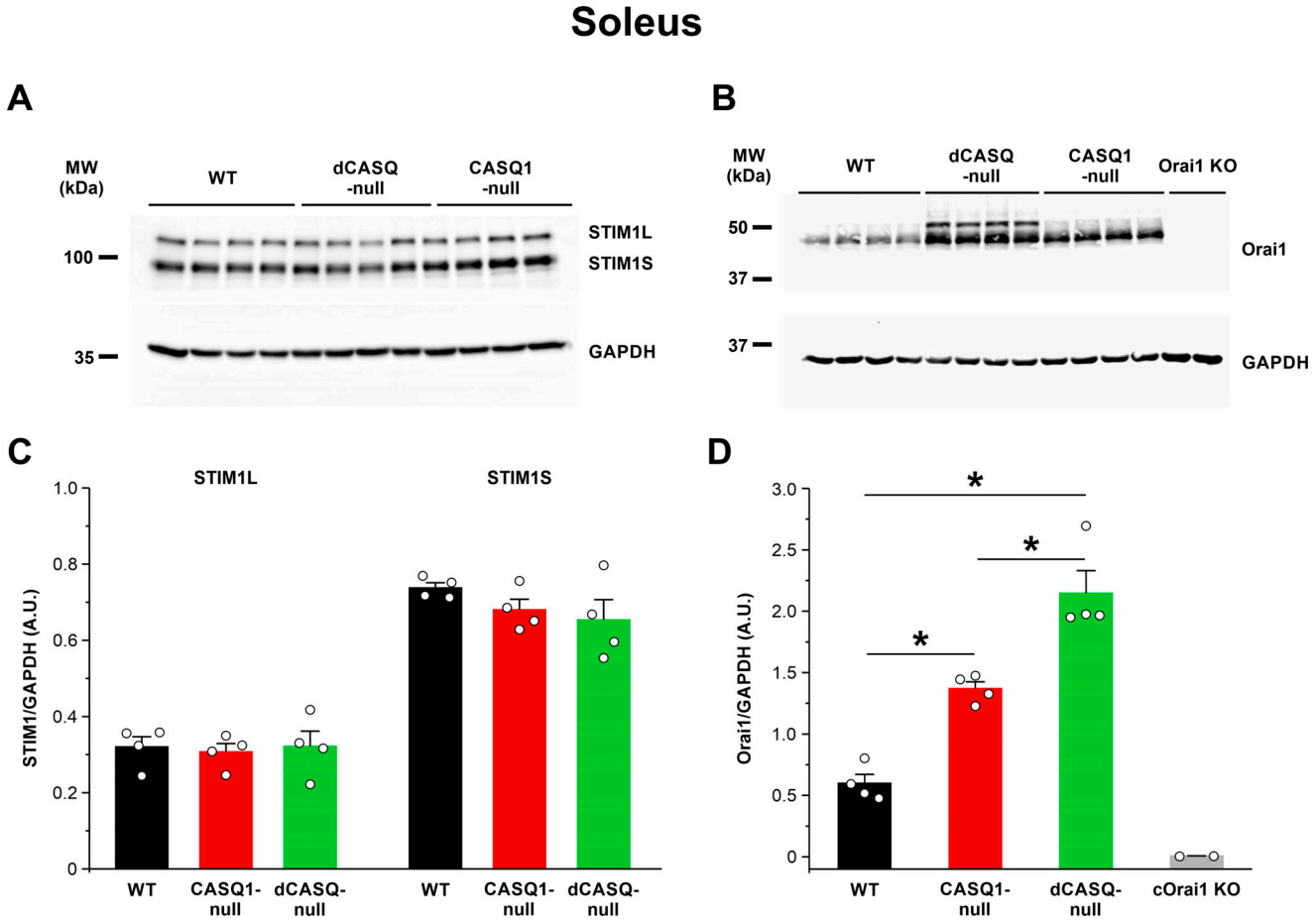

Figure 4. **Western blot analyses of proteins that coordinate SOCE in soleus muscle. (A and B)** Representative immunoblots showing expression levels of the long (STIM1L) and short (STIM1S) STIM1 splice variants (A) and Orai1 (B) in soleus muscle homogenates from WT (n = 4), CASQ1-null (n = 4), and dCASQ-null (n = 4) mice. For Orai1 expression, soleus muscles from constitutive, muscle-specific Orai1 KO (cOrai1 KO) mice were used as a negative control to validate the Orai1 antibody used. MW, molecular weight. **(C and D)** Relative band intensities (normalized to GAPDH) for each of the proteins shown in A and B. Data are shown as mean ± SEM. *, P = 0.0033, WT vs. CASQ1-null; *, P = 0.000017, WT vs. dCASQ-null; *, P = 0.0031, CASQ1-null vs. dCASQ-null. Source data are available for this figure: SourceData F4.

CEUs, and magnitude of SOCE, thus providing additional evidence that CEUs likely represent sites of Ca^{2+} entry through SOCE. In addition, our data indicate that in soleus muscle, (1) CASQ1, which represents the more abundant CASQ isoform, plays a key role in Ca^{2+} handling; and (2) CASQ2 alone is unable to fully compensate for loss of CASQ1. Together, these findings suggest that CASQ2 alone is able to partially mitigate the effects of CASQ1 ablation in soleus muscle and suggest that the two proteins exhibit redundant functions.

DL-specific force production during repetitive stimulation and both constitutive and maximum SOCE in single FDB fibers was not different between CASQ1- and dCASQ-null mice. In contrast, the additional KO of CASQ2 in CASQ1-null mice resulted in an even greater effect on soleus-specific force production during repetitive stimulation. Together, these results suggest that constitutive Ca^{2+} entry and SOCE would be expected to be further increased in soleus muscle fibers of dCASQ-null mice.

SOCE is activated in skeletal muscle during individual action potentials, a mode of SOCE referred to as pSOCE, because it showed kinetics comparable to EC coupling (Koenig et al., 2018; Koenig et al., 2019). In contrast to tonic SOCE, which represents a slower form of SOCE activation, pSOCE is proposed to occur within the triad junction during EC coupling, presumably activated by a local and transient depletion at the terminal cisternae of the SR Ca^{2+} stores. As one possibility, tonic SOCE might reflect constitutive Ca^{2+} influx occurring through CEUs (observed with acute exercise and CASQ deficiency), while pSOCE at the triad might provide an important pathway for Ca^{2+} influx during repetitive, high-frequency stimulation. However, a comprehensive assessment of this issue extends beyond the scope of the current study, and future experiments will be needed to more precisely unravel the function and subcellular location of tonic and phasic SOCE in skeletal muscle.

A limitation of this study is that we did not directly measure constitutive Ca^{2+} entry and SOCE in soleus muscle fibers. However, given the consistency of correlation between CEUs and the dependence of sustained contractility during repetitive stimulation in the presence of extracellular Ca^{2+}, it is reasonable to predict that both constitutive and maximum SOCE are

increased in soleus fibers from CASQ1-null mice and even more in soleus muscle fibers from dCASQ-null mice. Another limitation of this study is that we were unable to directly compare CEU properties between type I (~40%) and type IIA (~60%) fibers present in soleus muscle. From an ultrastructural point of view, type I and IIA fibers can be distinguished from each other based on specific structural features (i.e., Z-line width). However, since fiber type classification on this base is very difficult to achieve (the apparent Z-line width in the images is affected by section orientation), data for type I and IIA fibers were grouped together. However, (1) given that EDL muscle has virtually no type I fibers, while type I fibers represent ~40% of all fibers in the soleus muscle; (2) given the marked structural difference between type I/type IIA and type IIX/IIB fibers; and more importantly, (3) given that quantification of CEUs in soleus muscle did not exhibit a bimodal distribution, we may conclude that our EM measurements accurately assess the ultrastructure of type I and type IIA fibers in soleus muscles and type IIX/IIB fibers in EDL muscles. However, future studies that directly compare CEUs and both constitutive and maximum SOCE in type I and type IIA fibers are needed to provide a definitive conclusion.

The structure and size of CEUs are different between EDL and soleus fibers

In EDL fibers from exercised WT mice (Boncompagni et al., 2017), as well as those from sedentary CASQ1-null and dCASQ-null mice (Michelucci et al., 2020; Fig. S1), CEUs appear as a stack of multiple flat parallel membrane layers consisting of a single T-tubule extension from the triad associated with two or more layers of SR cisternae (Fig. 5). Detection of CEUs in soleus muscle fibers is more challenging. First, the I band of type I and type IIA fibers is usually occupied by mitochondria, which reduces the space available for assembly of stacks of longitudinal SR membranes (Fig. 5). More importantly, the relative total SR membrane surface and volume (junctional plus longitudinal SR) in soleus muscle fibers is ~30–40% smaller than that in EDL (Eisenberg et al., 1974; Luff and Atwood, 1971). As a logical consequence of this reduced SR surface/volume in soleus muscle fibers, a stack of SR cisternae forming CEUs would be expected to also be smaller (i.e., formed by fewer elements), similar to that observed for the jSR of the triad (Paolini et al., 2007).

Because CASQ1 deficiency leads to the constitutive assembly of CEUs in EDL muscle (Michelucci et al., 2020), we quantified CEUs in slow-twitch fibers of soleus muscle from both CASQ1-null and dCASQ-null mice. EM analyses of samples stained with ferrocyanide revealed that soleus fibers from both mouse lines contain a greater amount of long, thin, and convoluted T-tubule membranes within the I band that are not typically observed in soleus fibers from WT mice. In soleus fibers from dCASQ-null mice, T-tubule contact with the SR is greater than that observed in CASQ1-null mice, whereas no difference was found between the two CASQ-null genotypes in fast-twitch fibers of EDL muscle. High-magnification EM images revealed that elongated T-tubules in soleus muscle fibers are associated with SR elements to form T-tubule/SR stack junctions within the I band (CEUs). However, CEUs in soleus fibers are significantly smaller (i.e., formed by a lower number—one or two—of SR membrane elements) than that observed for CEUs in EDL muscle fibers (typically including more than two SR membrane elements; Boncompagni et al., 2017). This structural difference may also explain in part the different pattern of STIM1 expression in the two muscles. While expression of neither STIM1 splice variant is different in soleus muscles from WT, CASQ1-null, and dCASQ-null mice, expression of both STIM1S and STIM1L is significantly increased in EDL muscle of CASQ1-null and dCASQ-null mice compared with WT mice. Considering that the electron-dense strands of ~7–8 nm located within the CEU junctional gap (SR–SR and T-tubule/SR stack interfaces) may be constituted by STIM1 proteins (Boncompagni et al., 2017), the higher number of SR elements and the higher SR volume/surface in EDL muscle would be expected to correlate with greater STIM1 expression.

Orai1 expression, but not STIM1 expression, was increased in soleus muscles from CASQ1-null and even more in dCASQ-null mice, compared with WT mice

Although our results show that STIM1 expression was unaltered, Orai1 expression was increased approximately three- to fourfold in soleus muscle from CASQ1-null and dCASQ-null mice compared with WT mice. This increase in Orai1 expression is consistent with the observed increase in both total T-tubule length and T-tubule/SR stack contacts. Assuming Orai1 expression is limiting in skeletal muscle as expected, there is evidence to suggest that an increase in Orai1 expression would result in increased SOCE activity, even in the absence of a change in STIM1 expression. For example, an elegant study showed that Orai1 current density exhibits a highly nonlinear bell-shaped function of Orai1 expression at a constant level of STIM1 (Hoover and Lewis, 2011). Thus, a three- to fourfold increase in Orai1 expression could result in an increase in SOCE function even in the absence of a detectable change in STIM1 expression. Consistent with this, using a murine model of Duchenne muscular dystrophy in which SOCE activity is increased, several studies showed that this increase in SOCE correlates with a significant increment of Orai1 expression in the absence of a change in STIM1 expression (Edwards et al, 2010; Zhao et al, 2012; Goonasekera et al, 2014; García-Castañeda et al, 2022). However, other studies have reported a significant increase in STIM1S expression in muscles from *mdx* mice (Edwards et al., 2010; Cully et al., 2012).

Concluding remarks

Results presented in this study support the idea that T-tubule/SR stack junctions within the I band region of the sarcomere function as CEUs in both EDL and soleus muscles, strengthening the concept that CEUs represent sites of STIM1 and Orai1 coupling involved in constitutive Ca^{2+} entry and SOCE. Although the possibility that STIM1-Orai1 interact at other locations in skeletal muscle (e.g., triad) cannot be excluded, the results obtained in the current study and prior works (Boncompagni et al., 2017; Michelucci et al., 2019; Michelucci et al., 2020) suggest that the triad/Ca^{2+} release unit is not the primary location of functional STIM1-Orai1 coupling in skeletal muscle. On the other hand, T-tubule extensions within CEUs contain Orai1, and SR cisternae stack elements contain STIM1 (Boncompagni et al., 2017),

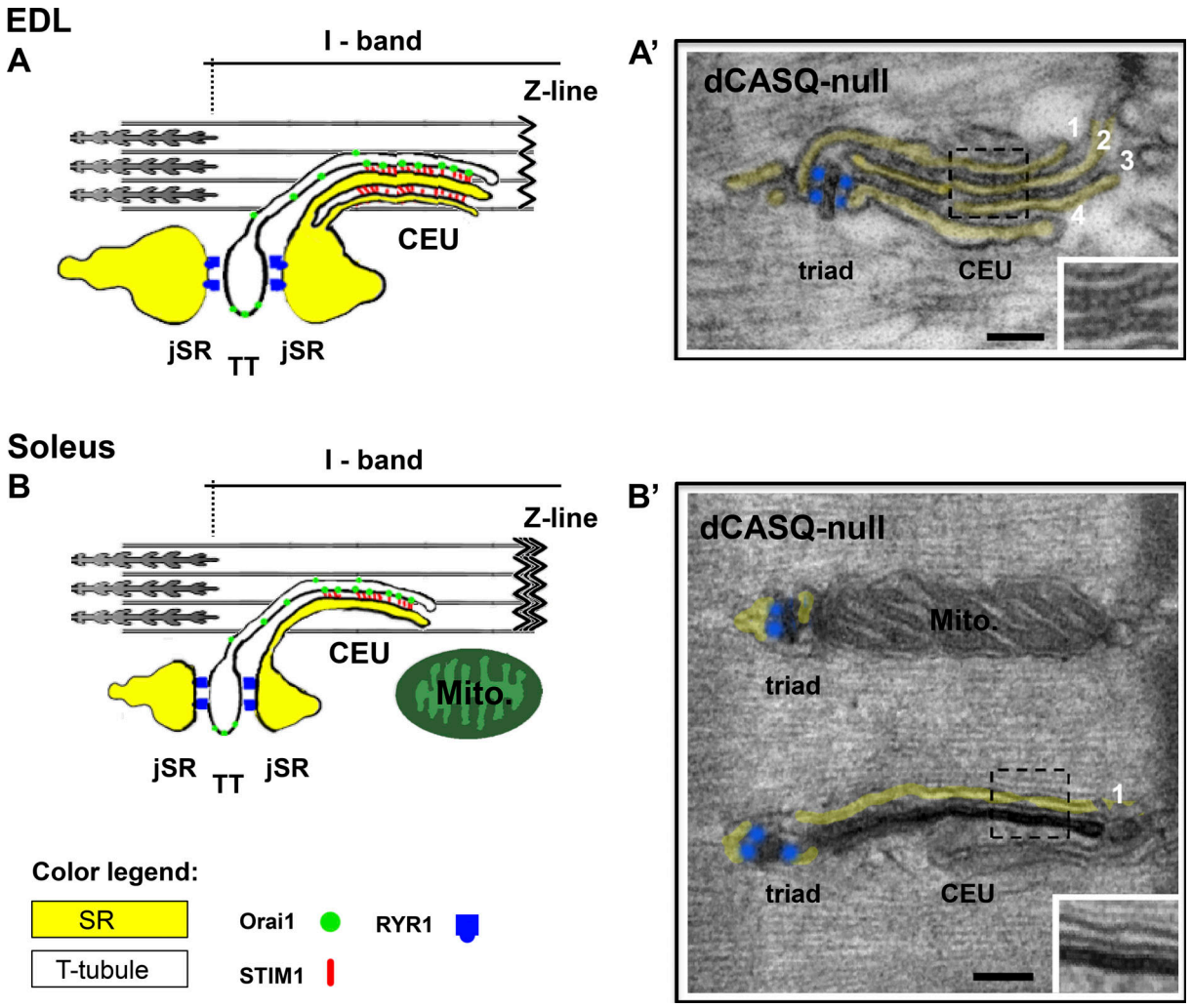

Figure 5. **Comparative models of CEUs in EDL and soleus fibers from WT mice and representative EM images of CEUs in EDL and soleus fibers from dCASQ-null mice. (A and B)** In adult mammalian fibers, the triad is placed approximately at the A-I band transition of the relaxed sarcomere. CEUs localize within the I band in close proximity to the triad, extending toward the Z-line. In soleus fibers, SR surface and volume are reduced compared with those of EDL fibers, and this difference is reflected in smaller triadic jSR, as well as in a lower number of longitudinal SR stack elements forming CEUs. **(A' and B')** In EDL muscle fibers from dCASQ-null mice, SR stacks of CEUs usually contain multiple SR membrane layers (four in the representative image in A'), while in soleus they typically contain one or two layers at the most (one in the representative image in B'). Within the junctional gap between both SR/SR membranes in the stack (dashed box and inset in A') and SR/T-tubule interface (dashed box and inset in B'), numerous and small electron-dense strands, likely reflecting STIM1 aggregates (Boncompagni et al., 2017), are visible. TT, T-tubule. Scale bar: 0.1 µm.

providing an ample area for STIM1-Orai1 interactions to account for the observed increase in SOCE activity and STIM1/Orai1 expression in muscle fibers from both CASQ1-null and dCASQ-null mice. Of course, these conclusions are based on indirect correlations between structural, functional, and biochemical data. In the absence of experimental approaches that provide a more direct measurement of constitutive and maximum SOCE within CEUs, we cannot conclude unequivocally that CEUs represent the only sites of functional STIM1 and Orai1 interactions in skeletal muscle.

An additional important finding of this study is that the incidence of CEU is inversely dependent on the expression level of CASQ proteins: the lower the expression of CASQ, the greater the number of CEUs per fiber area. Thus, CEUs, which are present at low levels both in soleus and EDL muscles of sedentary WT mice (Boncompagni et al., 2017; Protasi et al., 2021), are instead abundant in muscle of mice that lack CASQ, where SR Ca^{2+} buffer capacity is markedly decreased. Because the lumen of the SR throughout a muscle fiber is continuous (Lavorato et al., 2019), enabling fast equilibration of intra-SR [Ca^{2+}] as demonstrated in cardiac myocytes (Iyer et al., 2020), it is possible that the lumen of SR stacks within a CEU are in continuity with the lumen of the jSR of the triad, as it is clearly visible in thin EM sections (for example, see Fig. 5). This SR continuity between CEUs and jSR would create a preferential pathway for extracellular Ca^{2+} to refill nearby jSR needed to maintain SR Ca^{2+} release and muscle contractility during repetitive stimulation, especially when SR Ca^{2+} content and/or buffering capacity is limited. This could occur either during periods of intense/sustained muscle contraction, as is observed

in WT mice after acute exercise (Boncompagni et al., 2017; Michelucci et al., 2019), or when the Ca^{2+} buffer capacity within the SR is markedly reduced, as occurs in mice that are deficient of CASQ (Michelucci et al., 2020).

Acknowledgments

Eduardo Ríos served as editor.

This study was supported by grants from the National Institutes of Health: RO1 AR059646-06 subcontract to S. Boncompagni; AR059646 and R21 AR081068 to R.T. Dirksen; and AR059646 subcontract to F. Protasi.

The authors declare no competing financial interests.

Author contributions: A. Michelucci and S. Boncompagni conceived and directed the study. A. Michelucci designed and performed experiments, analyzed and interpreted data, and wrote/edited the manuscript; S. Boncompagni analyzed and interpreted data, provided resources, and wrote/edited the manuscript; L. Pietrangelo and G. Rastelli performed experiments and analyzed data; F. Protasi provided resources and CASQ1-null and dCASQ-null mice; and R.T. Dirksen provided resources and Orai1 knockout mice and edited the manuscript.

Submitted: 31 January 2022
Revised: 5 July 2022
Accepted: 27 July 2022

References

Armstrong, C.M., F.M. Bezanilla, and P. Horowicz. 1972. Twitches in the presence of ethylene glycol bis(-aminoethyl ether)-N, N′-tetracetic acid. *Biochim. Biophys. Acta*. 267:605–608. https://doi.org/10.1016/0005-2728(72)90194-6

Biral, D., P. Volpe, E. Damiani, and A. Margreth. 1992. Coexistence of two calsequestrin isoforms in rabbit slow-twitch skeletal muscle fibers. *FEBS Lett.* 299:175–178. https://doi.org/10.1016/0014-5793(92)80241-8

Boncompagni, S., R.E. Loy, R.T. Dirksen, and C. Franzini-Armstrong. 2010. The I4895T mutation in the type 1 ryanodine receptor induces fiber-type specific alterations in skeletal muscle that mimic premature aging. *Aging Cell*. 9:958–970. https://doi.org/10.1111/J.1474-9726.2010.00623.X

Boncompagni, S., A. Michelucci, L. Pietrangelo, R.T. Dirksen, and F. Protasi. 2017. Exercise-dependent formation of new junctions that promote STIM1-Orai1 assembly in skeletal muscle. *Sci. Rep.* 7:14286. https://doi.org/10.1038/s41598-017-14134-0

Boncompagni, S., A. Michelucci, L. Pietrangelo, R.T. Dirksen, and F. Protasi. 2018. Erratum: Addendum: Exercise-dependent formation of new junctions that promote STIM1-Orai1 assembly in skeletal muscle. *Sci. Rep.* 8:17463. https://doi.org/10.1038/s41598-018-33063-0

Canato, M., M. Scorzeto, M. Giacomello, F. Protasi, C. Reggiani, and G.J.M. Stienen. 2010. Massive alterations of sarcoplasmic reticulum free calcium in skeletal muscle fibers lacking calsequestrin revealed by a genetically encoded probe. *Proc. Natl. Acad. Sci. USA*. 107:22326–22331. https://doi.org/10.1073/pnas.1009168108

Cozens, B., and R.A. Reithmeier. 1984. Size and shape of rabbit skeletal muscle calsequestrin. *J. Biol. Chem.* 259:6248–6252. https://doi.org/10.1016/s0021-9258(20)82133-4

Cully, T.R., J.N. Edwards, O. Friedrich, D.G. Stephenson, R.M. Murphy, and B.S. Launikonis. 2012. Changes in plasma membrane Ca-ATPase and stromal interacting molecule 1 expression levels for Ca^{2+} signaling in dystrophic mdx mouse muscle. *Am. J. Physiol.. Cell Physiol.* 303: C567–C576. https://doi.org/10.1152/ajpcell.00144.2012

Damiani, E., and A. Margreth. 1994. Characterization study of the ryanodine receptor and of calsequestrin isoforms of mammalian skeletal muscles in relation to fibre types. *J. Muscle Res. Cell Motil.* 15:86–101. https://doi.org/10.1007/BF00130421

Damiani, E., P. Volpe, and A. Margreth. 1990. Coexpression of two isoforms of calsequestrin in rabbit slow-twitch muscle. *J. Muscle Res. Cell Motil.* 11: 522–530. https://doi.org/10.1007/BF01745219

Edwards, J.N., O. Friedrich, T.R. Cully, F. Von Wegner, R.M. Murphy, and B.S. Launikonis. 2010. Upregulation of store-operated Ca^{2+} entry in dystrophic mdx mouse muscle. *Am. J. Physiol. Cell Physiol.* 299:C42–C50. https://doi.org/10.1152/AJPCELL.00524.2009

Eisenberg, B.R., A.M. Kuda, and J.B. Peter. 1974. Stereological analysis of mammalian skeletal muscle. I. Soleus muscle of the adult guinea pig. *J. Cell Biol.* 60:732–754. https://doi.org/10.1083/JCB.60.3.732

Fliegel, L., E. Leberer, N.M. Green, and D.H. MacLennan. 1989. The fast-twitch muscle calsequestrin isoform predominates in rabbit slow-twitch soleus muscle. *FEBS Lett.* 242:297–300. https://doi.org/10.1016/0014-5793(89)80488-0

Franzini-Armstrong, C. 1970. Studies of the triad: I. structure of the junction in frog twitch fibers. *J. Cell Biol.* 47:488–499. https://doi.org/10.1083/JCB.47.2.488

Franzini-Armstrong, C., and A.O. Jorgensen. 1994. Structure and development of E-C coupling units in skeletal muscle. *Annu. Rev. Physiol.* 56: 509–534. https://doi.org/10.1146/annurev.ph.56.030194.002453

Franzini-Armstrong, C., F. Protasi, and V. Ramesh. 1999. Shape, size, and distribution of Ca^{2+} release units and couplons in skeletal and cardiac muscles. *Biophys. J.* 77:1528–1539. https://doi.org/10.1016/S0006-3495(99)77000-1

Froemming, G.R., B.E. Murray, S. Harmon, D. Pette, and K. Ohlendieck. 2000. Comparative analysis of the isoform expression pattern of Ca(2+)-regulatory membrane proteins in fast-twitch, slow-twitch, cardiac, neonatal and chronic low-frequency stimulated muscle fibers. *Biochim. Biophys. Acta*. 1466:151–168. https://doi.org/10.1016/S0005-2736(00)00195-4

García-Castañeda, M., A. Michelucci, N. Zhao, S. Malik, and R.T. Dirksen. 2022. Postdevelopmental knockout of Orai1 improves muscle pathology in a mouse model of Duchenne muscular dystrophy. *J. Gen. Physiol.* 154: 202213081. https://doi.org/10.1085/jgp.202213081

Goonasekera, S.A., J. Davis, J.Q. Kwong, F. Accornero, L. Wei-LaPierre, M.A. Sargent, R.T. Dirksen, and J.D. Molkentin. 2014. Enhanced Ca^{2+} influx from STIM1-Orai1 induces muscle pathology in mouse models of muscular dystrophy. *Hum. Mol. Genet*. 23:3706–3715. https://doi.org/10.1093/hmg/ddu079

Hoover, P.J., and R.S. Lewis. 2011. Stoichiometric requirements for trapping and gating of Ca^{2+} release-activated Ca^{2+} (CRAC) channels by stromal interaction molecule 1 (STIM1). *Proc. Natl. Acad. Sci. USA*. 108:13299–13304. https://doi.org/10.1073/PNAS.1101664108/-/DCSUPPLEMENTAL/PNAS.201101664SI

Ikemoto, N., G.M. Bhatnagar, B. Nagy, and J. Gergely. 1972. Interaction of divalent cations with the 55,000-dalton protein component of the sarcoplasmic reticulum. Studies of fluorescence and circular dichroism. *J. Biol. Chem.* 247:7835–7837. https://doi.org/10.1016/S0021-9258(19)44598-5

Iyer, K.A., Y. Hu, A.R. Nayak, N. Kurebayashi, T. Murayama, and M. Samsó. 2020. Structural mechanism of two gain-of-function cardiac and skeletal RyR mutations at an equivalent site by cryo-EM. *Sci. Adv.* 6: eabb2964. https://doi.org/10.1126/SCIADV.ABB2964

Koenig, X., R.H. Choi, and B.S. Launikonis. 2018. Store-operated Ca^{2+} entry is activated by every action potential in skeletal muscle. *Commun. Biol.* 1: 31. https://doi.org/10.1038/s42003-018-0033-7

Koenig, X., R.H. Choi, K. Schicker, D.P. Singh, K. Hilber, and B.S. Launikonis. 2019. Mechanistic insights into store-operated Ca^{2+} entry during excitation-contraction coupling in skeletal muscle. *Biochim. Biophys. Acta Mol. Cell Res.* 1866:1239–1248. https://doi.org/10.1016/J.BBAMCR.2019.02.014

Kurebayashi, N., and Y. Ogawa. 2001. Depletion of Ca^{2+} in the sarcoplasmic reticulum stimulates Ca^{2+} entry into mouse skeletal muscle fibres. *J. Physiol.* 533:185–199. https://doi.org/10.1111/j.1469-7793.2001.0185b.x

Lamboley, C.R.H., S.A.K. Guena, F. Touré, C. Hébert, L. Yaddaden, S. Nadeau, P. Bouchard, L. Wei-LaPierre, J. Lainé, E.C. Rousseau, et al. 2015. New method for determining total calcium content in tissue applied to skeletal muscle with and without calsequestrin. *J. Gen. Physiol.* 145: 127–153. https://doi.org/10.1085/JGP.201411250

Launikonis, B.S., and E. Ríos. 2007. Store-operated Ca^{2+} entry during intracellular Ca^{2+} release in mammalian skeletal muscle. *J. Physiol.* 583:81–97. https://doi.org/10.1113/jphysiol.2007.135046

Lavorato, M., R. Iyer, and C. Franzini-Armstrong. 2019. A proposed role for non-junctional transverse tubules in skeletal muscle as flexible segments allowing expansion of the transverse network. *Eur. J. Transl. Myol.* 29:8264. https://doi.org/10.4081/EJTM.2019.8264

Leberer, E., K.T. Härtner, and D. Pette. 1988. Postnatal development of Ca^{2+}-sequestration by the sarcoplasmic reticulum of fast and slow muscles in normal and dystrophic mice. *Eur. J. Biochem.* 174:247–253. https://doi.org/10.1111/J.1432-1033.1988.TB14090.X

Leberer, E., and D. Pette. 1986. Immunochemical quantification of sarcoplasmic reticulum Ca-ATPase, of calsequestrin and of parvalbumin in rabbit skeletal muscles of defined fiber composition. *Eur. J. Biochem.* 156: 489–496. https://doi.org/10.1111/J.1432-1033.1986.TB09607.X

Luff, A.R., and H.L. Atwood. 1971. Changes in the sarcoplasmic reticulum and transverse tubular system of fast and slow skeletal muscles of the mouse during postnatal development. *J. Cell Biol.* 51:369–383. https://doi.org/10.1083/JCB.51.2.369

Lyfenko, A.D., and R.T. Dirksen. 2008. Differential dependence of store-operated and excitation-coupled Ca^{2+} entry in skeletal muscle on STIM1 and Orai1. *J. Physiol.* 586:4815–4824. https://doi.org/10.1113/jphysiol.2008.160481

MacLennan, D.H., and P.T. Wong. 1971. Isolation of a calcium-sequestering protein from sarcoplasmic reticulum. *Proc. Natl. Acad. Sci. USA.* 68: 1231–1235. https://doi.org/10.1073/pnas.68.6.1231

Michelucci, A., S. Boncompagni, L. Pietrangelo, M. García-Castañeda, T. Takano, S. Malik, R.T. Dirksen, and F. Protasi. 2019. Transverse tubule remodeling enhances Orai1-dependent Ca^{2+} entry in skeletal muscle. *Elife.* 8:e47576. https://doi.org/10.7554/ELIFE.47576

Michelucci, A., S. Boncompagni, L. Pietrangelo, T. Takano, F. Protasi, and R.T. Dirksen. 2020. Pre-assembled Ca^{2+} entry units and constitutively active Ca^{2+} entry in skeletal muscle of calsequestrin-1 knockout mice. *J. Gen. Physiol.* 152:e202012617. https://doi.org/10.1085/JGP.202012617

Michelucci, A., M. García-Castañeda, S. Boncompagni, and R.T. Dirksen. 2018. Role of STIM1/ORAI1-mediated store-operated Ca^{2+} entry in skeletal muscle physiology and disease. *Cell Calcium.* 76:101–115. https://doi.org/10.1016/j.ceca.2018.10.004

Murphy, R.M., N.T. Larkins, J.P. Mollica, N.A. Beard, and G.D. Lamb. 2009. Calsequestrin content and SERCA determine normal and maximal Ca^{2+} storage levels in sarcoplasmic reticulum of fast- and slow-twitch fibres of rat. *J. Physiol.* 587:443–460. https://doi.org/10.1113/JPHYSIOL.2008.163162

Paolini, C., M. Quarta, A. Nori, S. Boncompagni, M. Canato, P. Volpe, P.D. Allen, C. Reggiani, and F. Protasi. 2007. Reorganized stores and impaired calcium handling in skeletal muscle of mice lacking calsequestrin-1. *J. Physiol.* 583:767–784. https://doi.org/10.1113/JPHYSIOL.2007.138024

Parekh, A.B., and J.W. Putney. 2005. Store-operated calcium channels. *Physiol. Rev.* 85:757–810. https://doi.org/10.1152/physrev.00057.2003

Protasi, F., L. Pietrangelo, and S. Boncompagni. 2021. Calcium entry units (CEUs): Perspectives in skeletal muscle function and disease. *J. Muscle Res. Cell Motil.* 42:233–249. https://doi.org/10.1007/s10974-020-09586-3

Putney, J.W. 1986. A model for receptor-regulated calcium entry. *Cell Calcium.* 7:1–12. https://doi.org/10.1016/0143-4160(86)90026-6

Ríos, E., M. Karhanek, J. Ma, and A. González. 1993. An allosteric model of the molecular interactions of excitation-contraction coupling in skeletal muscle. *J. Gen. Physiol.* 102:449–481. https://doi.org/10.1085/jgp.102.3.449

Ríos, E., G. Pizarro, and E. Stefani. 1992. Charge movement and the nature of signal transduction in skeletal muscle excitation-contraction coupling. *Annu. Rev. Physiol.* 54:109–133. https://doi.org/10.1146/annurev.ph.54.030192.000545

Royer, L., M. Sztretye, C. Manno, S. Pouvreau, J. Zhou, B.C. Knollmann, F. Protasi, P.D. Allen, and E. Ríos. 2010. Paradoxical buffering of calcium by calsequestrin demonstrated for the calcium store of skeletal muscle. *J. Gen. Physiol.* 136:325–338. https://doi.org/10.1085/JGP.201010454

Sacchetto, R., P. Volpe, E. Damiani, and A. Margreth. 1993. Postnatal development of rabbit fast-twitch skeletal muscle: Accumulation, isoform transition and fibre distribution of calsequestrin. *J. Muscle Res. Cell Motil.* 14:646–653. https://doi.org/10.1007/BF00141561

Schneider, M.F. 1994. Control of calcium release in functioning skeletal muscle fibers. *Annu. Rev. Physiol.* 56:463–484. https://doi.org/10.1146/annurev.ph.56.030194.002335

Schneider, M.F., and W.K. Chandler. 1973. Voltage dependent charge movement of skeletal muscle: A possible step in excitation-contraction coupling. *Nature.* 242:244–246. https://doi.org/10.1038/242244a0

Stiber, J., A. Hawkins, Z.S. Zhang, S. Wang, J. Burch, V. Graham, C.C. Ward, M. Seth, E. Finch, N. Malouf, et al. 2008. STIM1 signalling controls store-operated calcium entry required for development and contractile function in skeletal muscle. *Nat. Cell Biol.* 10:688–697. https://doi.org/10.1038/ncb1731

Sztretye, M., J. Yi, L. Figueroa, J. Zhou, L. Royer, and E. Ríos. 2011. D4cpv-calsequestrin: A sensitive ratiometric biosensor accurately targeted to the calcium store of skeletal muscle. *J. Gen. Physiol.* 138:211–229. https://doi.org/10.1085/jgp.201010591

Wei-Lapierre, L., E.M. Carrell, S. Boncompagni, F. Protasi, and R.T. Dirksen. 2013. Orai1-dependent calcium entry promotes skeletal muscle growth and limits fatigue. *Nat. Commun.* 4:2805. https://doi.org/10.1038/NCOMMS3805

Zhao, X., J.G. Moloughney, S. Zhang, S. Komazaki, and N. Weisleder. 2012. Orai1 mediates exacerbated Ca^{2+} entry in dystrophic skeletal muscle. *PLoS One.* 7:e49862. https://doi.org/10.1371/journal.pone.0049862

Ziman, A.P., C.W. Ward, G.G. Rodney, W.J. Lederer, and R.J. Bloch. 2010. Quantitative measurement of Ca^{2+} in the sarcoplasmic reticulum lumen of mammalian skeletal muscle. *Biophys. J.* 99:2705–2714. https://doi.org/10.1016/j.bpj.2010.08.032

Zitt, C., B. Strauss, E.C. Schwarz, N. Spaeth, G. Rast, A. Hatzelmann, and M. Hoth. 2004. Potent inhibition of Ca^{2+} release-activated Ca^{2+} channels and T-lymphocyte activation by the pyrazole derivative BTP2. *J. Biol. Chem.* 279:12427–12437. https://doi.org/10.1074/JBC.M309297200

Supplemental material

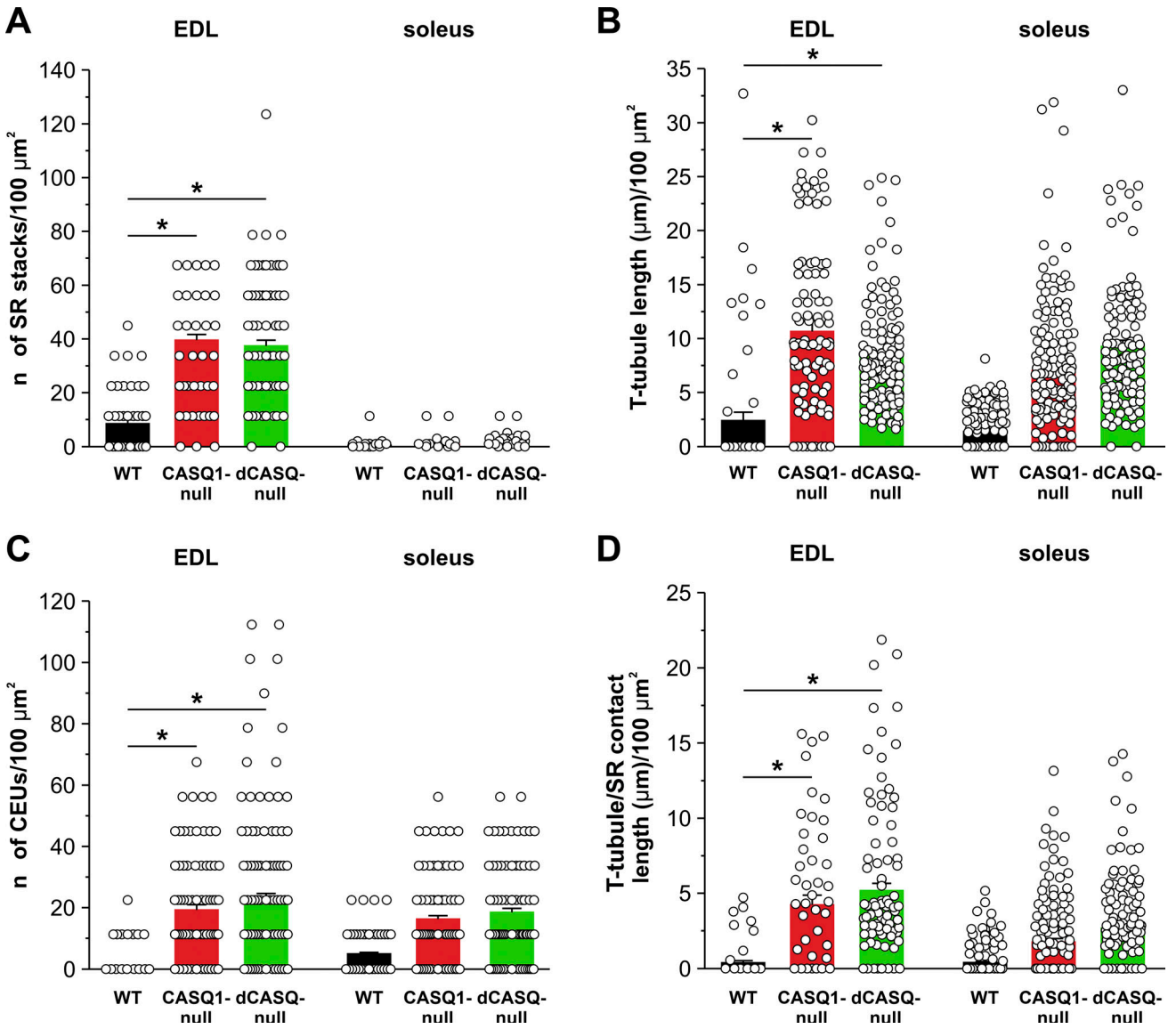

Figure S1. **Comparison of the incidence of SR stacks and CEUs, T-tubule extensions, and T-tubule/SR stack contact length between EDL and soleus muscle fibers. (A–D)** Quantitative analyses of the number of SR stacks per 100 µm² of cross-sectional area (A), T-tubule length in the I band (µm/100 µm² of cross-sectional area; B), the number of CEUs per 100 µm² of cross-sectional area (C), and length of T-tubule/SR stack contacts in the I band (expressed as µm/100 µm² of cross sectional area; D) determined from cross sections of EDL (left bars) muscle fibers from WT (n = 60; n = 60; n = 112; n = 60 fibers), CASQ1-null (n = 150; n = 100; n = 100; n = 53 fibers), and dCASQ-null (n = 104; n = 123; n = 145; n = 103 fibers) mice. Right bars in each plot represent the soleus muscle fibers from WT, CASQ1-null, and dCASQ-null mice shown in Fig. 2. Data are shown as mean ± SEM. Statistical analysis for EDL muscle fibers: A: *, P = 0.000000038, WT vs. CASQ1-null; *, P = 0.000000029, WT vs. dCASQ1-null. B: *, P = 0.000000028, WT vs. CASQ1-null. *, P = 0.000000024, WT vs. dCASQ-null. C: *, P = 0.000000027 WT vs. CASQ1-null; *, P = 0.000000013 WT vs. dCASQ-null. D: *, P = 0.0000064, WT vs. CASQ1-null; *, P = 0.000000027, WT vs. dCASQ-null. Number of mice used: WT, n = 3; CASQ1-null, n = 3; dCASQ-null, n = 3. Note: quantitative EM analyses of SR stacks per 100 µm² of cross-sectional area (A), T-tubule length in the I band (µm/100 µm² of cross-sectional area; B), and length of T-tubule/SR contacts in the I band in EDL muscles from WT and CASQ1-null mice (D) were replotted from Michelucci et al. (2020).

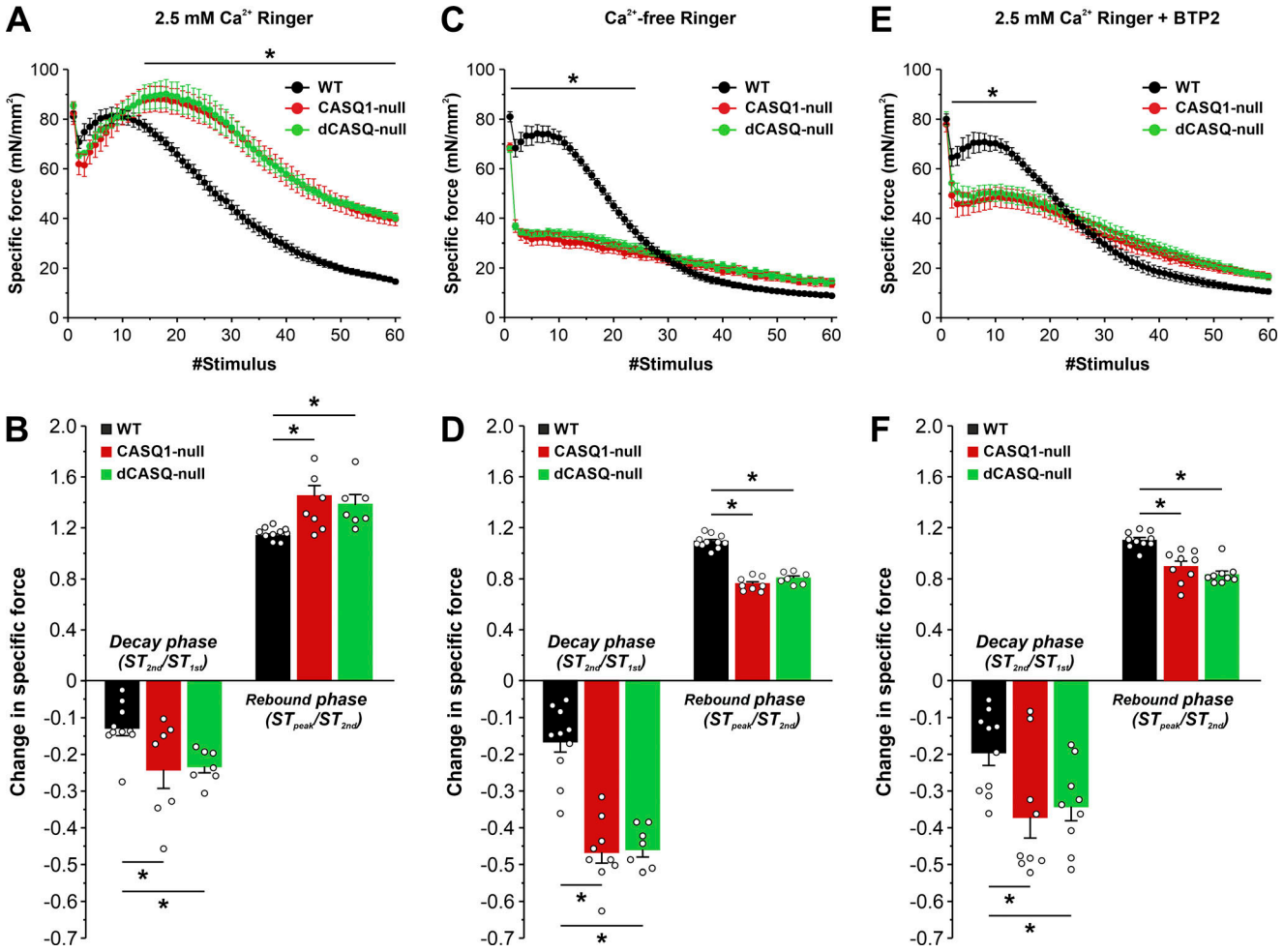

Figure S2. **Ca^{2+} influx dependence of contractile force during repetitive high-frequency stimulation of intact EDL muscles. (A, C, and E)** Time course of peak specific force in EDL muscles from WT (A and B, *n* = 11; C and D, *n* = 10; E and F, *n* = 10 muscles), CASQ1-null (A and B, *n* = 7; C and D, *n* = 9; E and F, *n* = 9 muscles), and dCASQ-null (A and B, *n* = 7; C and D, *n* = 7; E and F, *n* = 9 muscles) mice during 60 consecutive 500-ms-duration stimulus trains in the presence of either standard Ringer's solution containing 2.5 mM Ca^{2+} (A), nominally Ca^{2+}-free Ringer's solution (C), or standard Ringer's solution supplemented with 10 µM BTP2 (E). **(B, D, and F)** Quantitative analyses of the relative decay during the second stimulus train (ST_{2nd}/ST_{1st}) and the peak of the rebound phase (ST_{peak}/ST_{2nd}) from the corresponding data shown in A, C, and E. Data are shown as mean ± SEM. Statistical analysis: B, decay phase: *, P = 0.039, WT vs. CASQ1-null; *, P = 0.044, WT vs. dCASQ-null; rebound phase: *, P = 0.018, WT vs. CASQ1-null; *, P = 0.02, WT vs. dCASQ-null. D, decay phase: *, P = 0.000000065, WT vs. CASQ1-null; *, P = 0.00000021, WT vs. dCASQ-null; rebound phase: *, P = 0.000000000027, WT vs. CASQ1-null; *, P = 0.0000000025, WT vs. dCASQ-null. F, decay phase: *, P = 0.022, WT vs. CASQ1-null; *, P = 0.046, WT vs. dCASQ-null; rebound phase: *, P = 0.00015, WT vs. CASQ1-null; *, P = 0.0000031, WT vs. dCASQ-null. Number of mice used: WT (A and B, *n* = 8; C and D, *n* = 8; E and F, *n* = 7), CASQ1-null (A and B, *n* = 4; C and D, *n* = 5; E and F, *n* = 7); dCASQ-null (A and B, *n* = 4; C and D, *n* = 5; E and F, *n* = 6).

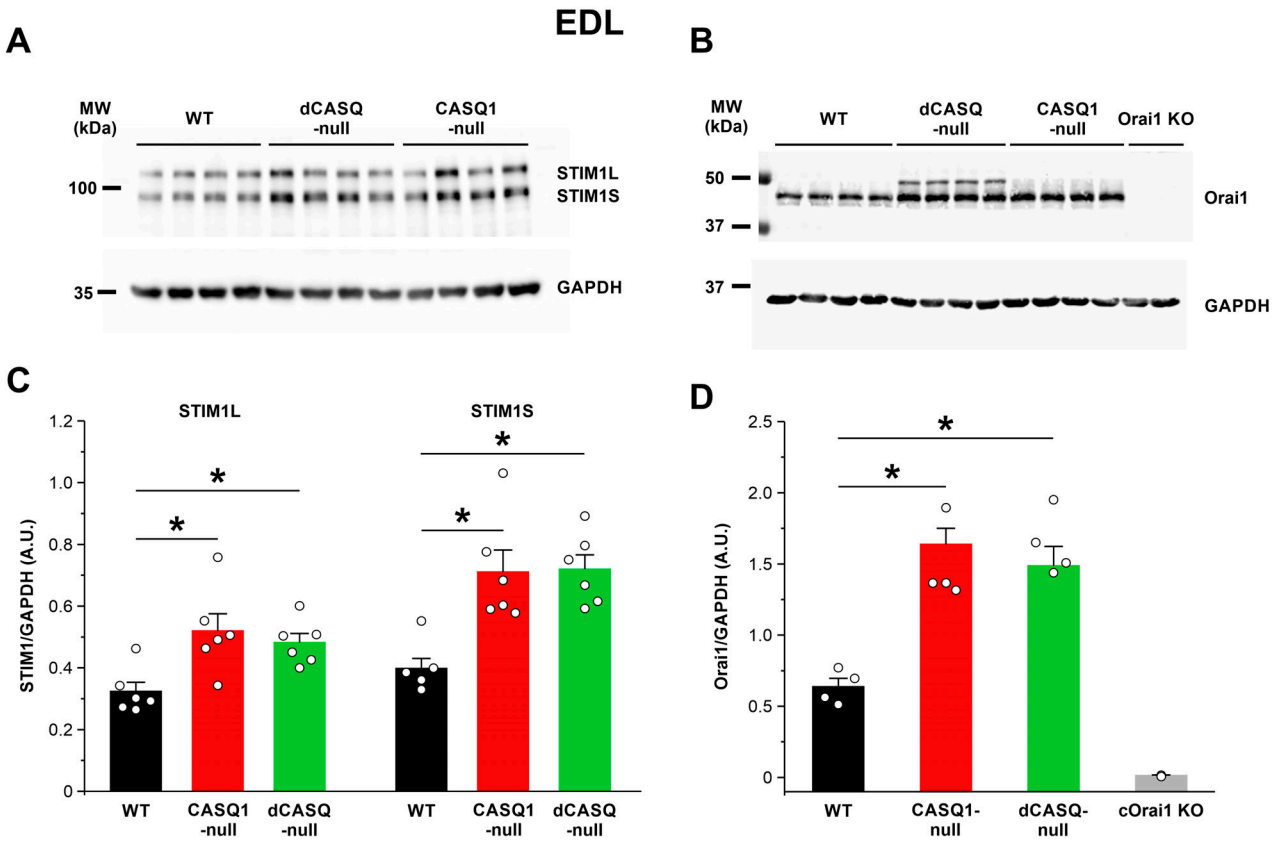

Figure S3. **Western blot analyses of proteins that coordinate SOCE in EDL muscle. (A and B)** Representative immunoblots showing expression levels of the long (STIM1L) and short (STIM1S) STIM1 splice variants (A) and Orai1 (B) in EDL muscle homogenates from WT (n = 6, C; n = 4, D), CASQ1-null (n = 6, C; n = 4, D), and dCASQ-null (n = 6, C; n = 4, D) mice. For Orai1 expression, EDL muscles from constitutive, muscle-specific Orai1 KO (cOrai1 KO) mice (n = 2) were used as a negative control to validate the Orai1 antibody used. **(C and D)** Relative band intensities (normalized to GAPDH) for each of the proteins shown in A and B. Data are shown as mean ± SEM. Statistical significance: C: *, P = 0.0095 and *, P = 0.002 for STIM1L and STIM1S, respectively, WT vs. CASQ1-null; *, P = 0.04 and *, P = 0.0016 for STIM1L and STIM1S, respectively, WT vs. dCASQ-null; D: *, P = 0.00093, WT vs. CASQ1-null; *, P = 0.00028, WT vs. dCASQ-null. Source data are available for this figure: SourceData FS3.

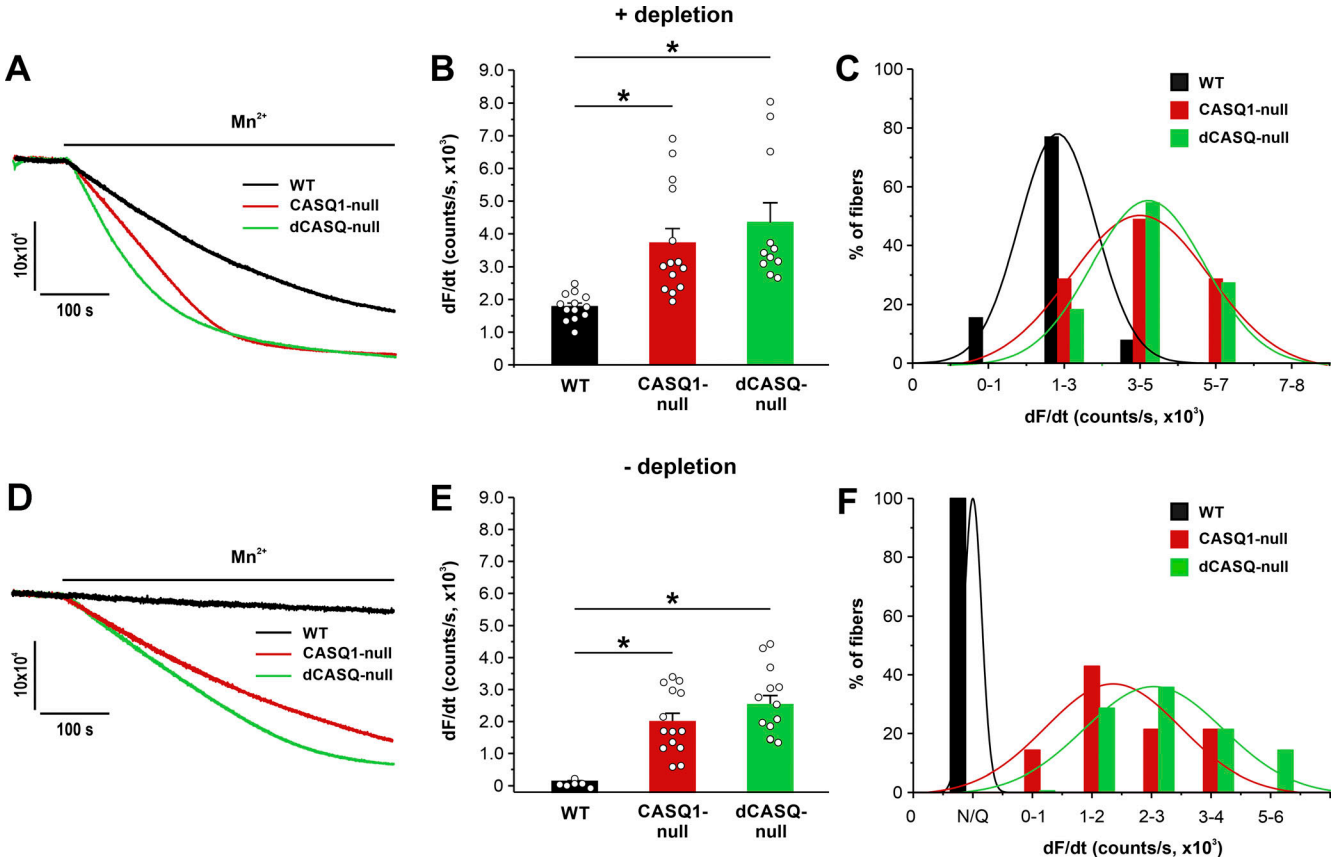

Figure S4. **Maximum rate of Mn^{2+} quench in FDB fibers in the presence or absence of pharmacological SR Ca^{2+} store depletion. (A)** Representative traces of fura-2 fluorescence during application of 0.5 mM Mn^{2+} recorded in FDB fibers isolated from WT (*n* = 13 fibers), CASQ1-null (*n* = 14 fibers), and dCASQ-null (*n* = 11 fibers) mice following store depletion with 1 µM thapsigargin and 15 µM cyclopiazonic acid (+depletion, i.e., maximum SOCE). **(B)** Quantitative analyses of the maximum rate of Mn^{2+} quench in store-depleted fibers. **(C)** Frequency histogram of percentage of FDB fibers exhibiting different levels of maximal rate of Mn^{2+} quench. **(D)** Representative traces of fura-2 fluorescence during application of 0.5 mM Mn^{2+} recorded in FDB fibers isolated from WT (*n* = 7 fibers), CASQ1-null (*n* = 14 fibers), and dCASQ-null (*n* = 14 fibers) mice in the absence of store depletion (–depletion, i.e., constitutive SOCE). **(E)** Quantitative analyses of the maximum rate of Mn^{2+} quench in the absence of store depletion. **(F)** Frequency histogram of percentage of FDB fibers exhibiting different levels of maximal rate of Mn^{2+} quench. Data are shown as mean ± SEM. Statistical significance: B: *, P = 0.0052, WT vs. CASQ1-null; *, P = 0.0005, WT vs. dCASQ-null; F: *, P = 0.00024, WT vs. CASQ1-null; *, P = 0.0000064, WT vs. dCASQ-null. Number of mice used: WT (*n* = 4); CASQ1-null (*n* = 5); dCASQ-null (*n* = 4).